



OPEN

Radiation synthesis and chemical modifications of p(AAm-co-AAc) hydrogel for improving their adsorptive removal of metal ions from polluted water

Israa Kamal Abdel Maksoud¹, Ghada Bassioni², Norhan Nady³, Sherif A. Younis⁴✉, Mohamed Mohamady Ghobashy⁵✉ & M. S. A. Abdel-Mottaleb¹

The research focuses on utilizing gamma irradiation to synthesize polyacrylic acid-co-polyacrylamide p(AAm-co-AAc) hydrogels. The effect of synthetic parameters on physicochemical features of p(AAm-co-AAc) hydrogels were examined, including acrylic acid (AAc): acrylamide (AAm) weight ratios, monomer concentration, and gamma irradiation dosage (kGy). At the optimum synthetic conditions (30 kGy and 75% AAc), different chemical modifications are explored to incorporate sulfonate, hydroxyl, carboxyl, cysteine, thiol, and amine functional groups within the bare hydrogel (Cpd 0) structure. Fourier-transform infrared spectroscopy (FTIR) and scanning electron microscopy (SEM) analyses confirmed the successful development of functionalized hydrogels (namely Cpd 1 to 6) with three-dimensional porous structures. These modified hydrogels include Cpd 1, a sulfonated hydrogel through a sulfonation reaction; Cpd 2, modified via NaOH hydrolysis; Cpd 3, modified using thionyl chloride; Cpd 4, incorporating cysteine modification through reaction with cysteine; Cpd 5, with 4-(Dimethylamino) benzaldehyde; and Cpd 6, modified with 3,4-Dimethylbenzoic acid. The effect of hydrogel composition and surface functionalities on the swelling capacity and interactions with scale-forming/heavy metal ions (e.g., Ba²⁺, Sr²⁺, and Cu²⁺) was investigated in saline water solution (NaCl = 1000 mg/L). Batch adsorption studies reveal that all modified hydrogels exhibited higher removal efficiency for the three metal ions than unmodified p(AAm-co-AAc) hydrogel, validating the key role of surface functionalities in tailoring hydrogel affinity for metal ions adsorption. Amongst these, NaOH-treated hydrogel (Cpd 2) outperformed all other modified ones in the removal of Cu²⁺, Ba²⁺, and Sr²⁺ ions, with maximum capacities of 13.67, 36.4, and 27.31 mg/g, respectively. Based on adsorption isotherm and kinetic modeling, the adsorption process of the three metal ions onto all modified hydrogels better obeyed Freundlich isotherm and pseudo-first-order kinetic models. Thermodynamic studies also indicated that the adsorption behavior of Sr²⁺ ions can exhibit both exothermic and endothermic characteristics, depending on the nature of hydrogel surface chemistry. Conversely, the adsorption process of Cu²⁺ and Ba²⁺ ions onto all modified hydrogels is endothermic, suggesting favorable chemical adsorption mechanisms. These findings reveal that the specific adsorption performance of hydrogel is dependent on the type of modification and the targeted heavy metal ions. Based on the nature of hydrogel surface functionality, surface modifications can change the charge density, hydrophilicity, and overall chemical environment of the hydrogel, offering a versatile approach to optimize the adsorption affinity/selectivity of hydrogel's in removing scale-forming/heavy metals from water solutions.

¹Department of Chemistry, Faculty of Science, Ain Shams University, Abbassia, Cairo 11566, Egypt. ²Department of Physics and Engineering Mathematics, Faculty of Engineering, Ain Shams University, Cairo, Egypt. ³Polymeric Materials Research Department, Advanced Technology and New Materials Research Institute, City of Scientific Research and Technological Applications (SRTA-City), New Borg El-Arab City, Alexandria 21934, Egypt. ⁴Analysis and Evaluation Department, Egyptian Petroleum Research Institute (EPRI), Nasr City, Cairo 11727, Egypt. ⁵Radiation Research of Polymer Department. National Center for Radiation Research and Technology (NCRRT), Egyptian Atomic Energy Authority (EAEA), Cairo, Egypt. ✉email: sherifali_r@yahoo.com; Mohamed_ghobashy@yahoo.com

The growth of industries has played a vital role in advancing society, improving living standards, and driving economic development¹. However, this industrial progress has come at a cost with the increased pollution of water bodies that poses significant risks to the environment and living organisms². In particular, releasing heavy metal ions into water sources has become a considerable concern and a pressing issue that requires immediate attention³. In particular, copper (Cu^{2+}), barium (Ba^{2+}), and strontium (Sr^{2+}) ions are among the toxic heavy metals on human health and the environment. The World Health Organization (WHO) has established maximum permissible limits for these ions in drinking water at 2 mg/L for Cu^{2+} , 0.7 mg/L for Ba^{2+} , and 1.5 mg/L for Sr^{2+} ⁴. Copper contamination in aquatic ecosystems can adversely affect marine organisms, disrupting their physiological processes and overall ecosystem balance⁵. The toxicity of barium primarily depends on its cumulative health effects, including kidney damage and neurological disorders⁶. Strontium is a naturally occurring element in rocks, soil, and water. While strontium is not highly toxic, specific forms, like radioactive strontium-90, can pose serious health risks. Radioactive strontium-90 can enter the food chain through contaminated water and soil, leading to increased risks of cancer, particularly bone cancer⁷. These toxic metal ions can be found in various sources like pesticides, fungicides, refineries, fertilizers, mining activities, smoking, nuclear fission plants, chemical industries, paints, electroplating, welding, automobiles, batteries, and many others⁸. Their contamination of water bodies can harm aquatic ecosystems and pose serious health risks to humans⁹.

Over the past decades, numerous research efforts have been devoted to developing efficient methods for removing toxic ions from water to address this challenge in recent years. Among the various approaches available, adsorption has emerged as a promising technique due to its effectiveness, scalability, and versatility¹⁰. Adsorption involves the attachment of pollutants to the surface of a solid material, known as an adsorbent, thereby removing them from the water¹¹. For instance, different adsorbent materials (e.g., polymeric, carbon, metal oxides, hybrid metal–organic composite, etc.) have been prepared and proposed for heavy/toxic metal ion adsorption. Amongst, polymeric hydrogels have recently emerged as promising adsorbent materials for removing heavy/poisonous metal ions from water due to their unique properties, including high porosity and hydrophilicity¹². Specifically, polymeric hydrogels with 3D networking structures have gained considerable attention for effectively removing metal ions from different types of wastewater¹³. The 3D polymeric hydrogels are formed through crosslinking hydrophilic polymers, resulting in a network with high porosity, surface functionality, and capacitance to uptake water contaminants (i.e., via swelling properties). Hydrogels demonstrated multiple advantages, such as the highly hydrophilic nature with many polar surface functionalities that accelerate the formation of electrostatic and coordination bonds with heavy metal cations¹⁴. Hydrogels are generally non-toxic with good biocompatibility, making them suitable for environmental applications¹⁵.

For hydrogel synthesis, the radiation technique is recognized as a valuable method for crosslinked hydrogel^{16,17} to be used as a template¹⁸, semi-permeable membrane¹⁹, and blend polymer²⁰ based on green renewable resources to protect the environment from harmful effects^{21–23}. Hydrogels-based renewable biopolymers have also attracted considerable research interest for potential applications in environmental remediation, such as wastewater treatment and pollution protection²⁴. Since the surface chemistry (specifically, the functional chelating entities) of the polymer matrix is primarily responsible for the hydrogel's ability to remove metal, it is also possible to modify the monomer structure during in-situ polymerization and change the surface functional moieties ex-situ using chemical modification techniques. In this respect, many efforts have been made to incorporate various surface functionalities (such as sulfonic, hydroxyl, phosphate, carboxylic acid, amine/amide, and epoxy moieties) on hydrogel adsorbents to increase their adsorption affinity for heavy metal cations through complexation and electrostatic interaction mechanisms^{25,26}. For instance, acrylamide (AAm) and acrylic acid (AAc) are the most common monomers synthesizing hydrogel adsorbents to remove metal ions²⁷. Using AAm and AAc monomers, graft copolymerization reaction of poly (acrylamide-co-acrylic acid) hydrogel was carried out to involve carboxyl surface functionalities for enhanced adsorption removal of some heavy metals (e.g., Cr^{2+} , Cu^{2+} , Ni^{2+} , and Zn^{2+})²⁸. By copolymerizing acrylic acid (AA) and sodium styrene sulfonate (SS), modified carboxymethyl cellulose (CMC)-based hydrogels with sulfonate groups ($-\text{SO}_3\text{Na}$) were also created for efficient removal of Cu^{2+} and Zn^{2+} ions²⁹. However, it should be noted that three crucial factors, including (i) the polymer volume fraction of hydrogel, (ii) the degree of cross-linking, and (iii) the size of the network mesh, could affect the metal capacity of radiation-induced-graft polymeric adsorbents. These variables affect the swelling ratio (the amount of absorbed water), mechanical strength, and the diffusivity of reactant molecules (heavy metal ions) into the hydrogel structure. This in turn affects the stability, toughness, and capacitance of the adsorbent during water treatment.

On the above basis, this research article aims to provide a comprehensive study of using the radiation-induced synthesis method to prepare hydrogel-based adsorbents with different functionalities to effectively remove metal ions (e.g., Cu^{2+} , Ba^{2+} , and Sr^{2+} ions) from water bodies. The chosen gamma irradiation will be selected to control the crosslinking polymerization of acrylamide (AAm) and acrylic acid (AAc) chains, forming a 3D (AAc-co-AAm) hydrogel network with high porosity and swelling capacity. Hence, the gamma radiation synthesis approach will include optimizing irradiation parameters based on the characteristics of the resulting hydrogels. The best hydrogel with the highest swelling capacitance will further be selected for different chemical modification strategies to introduce sulfonate, carboxyl, thiol, hydroxyl, and amine groups that effectively chelate and exchange metal ions from natural and low-saline water solution (at 1000 mg/L NaCl). The hydrogel chelation and ion exchange properties will also be evaluated through batch experiments as a function of operating parameters like temperature, contact time (t), initial metal ions (Cu^{2+} , Ba^{2+} , and Sr^{2+}) concentrations, solution pH, and hydrogel dosage. Finally, the prospects in hydrogel-based adsorbents for metal ions removal will be discussed, highlighting potential research directions and emerging technologies. The novelty of this study lies in developing a hydrogel with excellent chelation and ion exchange capabilities for removing heavy and toxic metals from water, explicitly focusing on Cu^{2+} , Ba^{2+} , and Sr^{2+} ions. The adsorption mechanisms involved in the interaction among ions and hydrogel-based adsorbents will be examined, shedding light on the factors influencing adsorption capacity, selectivity, isotherms, thermodynamics, and kinetics.

Experimental methods experimental

Materials

Acrylic acid (AA) and acrylamide (AAm) monomers (99%, analytical grade) were purchased from Fluka Co., Germany. Sulfanilic acid, thionyl chloride (SOCl₂), cysteine with 4-(Dimethylamino) benzaldehyde, and 3,4-Dimethylbenzoic acid were supplied as analytical grade chemicals (> 97% purity) from Sigma-Aldrich. Sodium hydroxide (NaOH: 98%) and Sodium chloride (NaCl: 99%) were purchased from ADWICK™ commercial.

Preparation of p(AAm-co-AAc) hydrogel for metal ions removal.

The synthesis procedure of hydrogel consisting of crosslinked polyacrylic acid and polyacrylamide networks using the gamma irradiation technique is shown in Fig. 1. In this procedure, different volume-to-weight ratios (12, 22, or 27 v/wt %) of acrylic acid (AAc: 1.25, 2.3, or 2.8 mL) and acrylamide (AAm: 3.75, 6.9, or 8.5 g) comonomers was dissolved in 40 mL of deionized (DI) water. The obtained AAc/AAm solution mixtures were subject to a gamma-ray dose of 10 kGy. Different comonomer compositions of (AAc/AAm) at v/wt% of (25/75), (50/50), and (25/75) have been prepared at the gamma-ray dose of 10 kGy. Swelling and gel fraction experiments tested the prepared hydrogel samples of p(AAm-co-AAc) to a candidate for the best comonomers compositions to study the impact of irradiation doses. The effect of irradiation doses on the swelling and gel fraction of p(AAm-co-AAc) was carried out at 10, 20, and 30 kGy.

Chemical modification of p(AAm-co-AAc) hydrogel

Different chemical modification strategies were carried out to functionalize the bare p(AAm-co-AAc) hydrogel (coded as Cpd 0) with thiol (-SH), amino (-NH₂), or carboxyl (-COOH), allowing the development of six functional hydrogels (coded as Cpd 1 to Cpd 6). These functional groups can selectively bind and remove the target ions from the solution. The chemical modification scheme of Cpd 0 to prepare modified Cpd 1 to Cpd 6 is illustrated in Fig. 1.

Reaction with sulfanilic acid

Dispersal 1.5 g of p(AAm-co-AAc) hydrogel sample (Cpd 0) is reacted with NaOH at a temperature of 90 °C. The obtained sample was dispersed in 120 mL of water containing 1.25 mol of sulfanilic acid (Fig. 1). The hydrogel

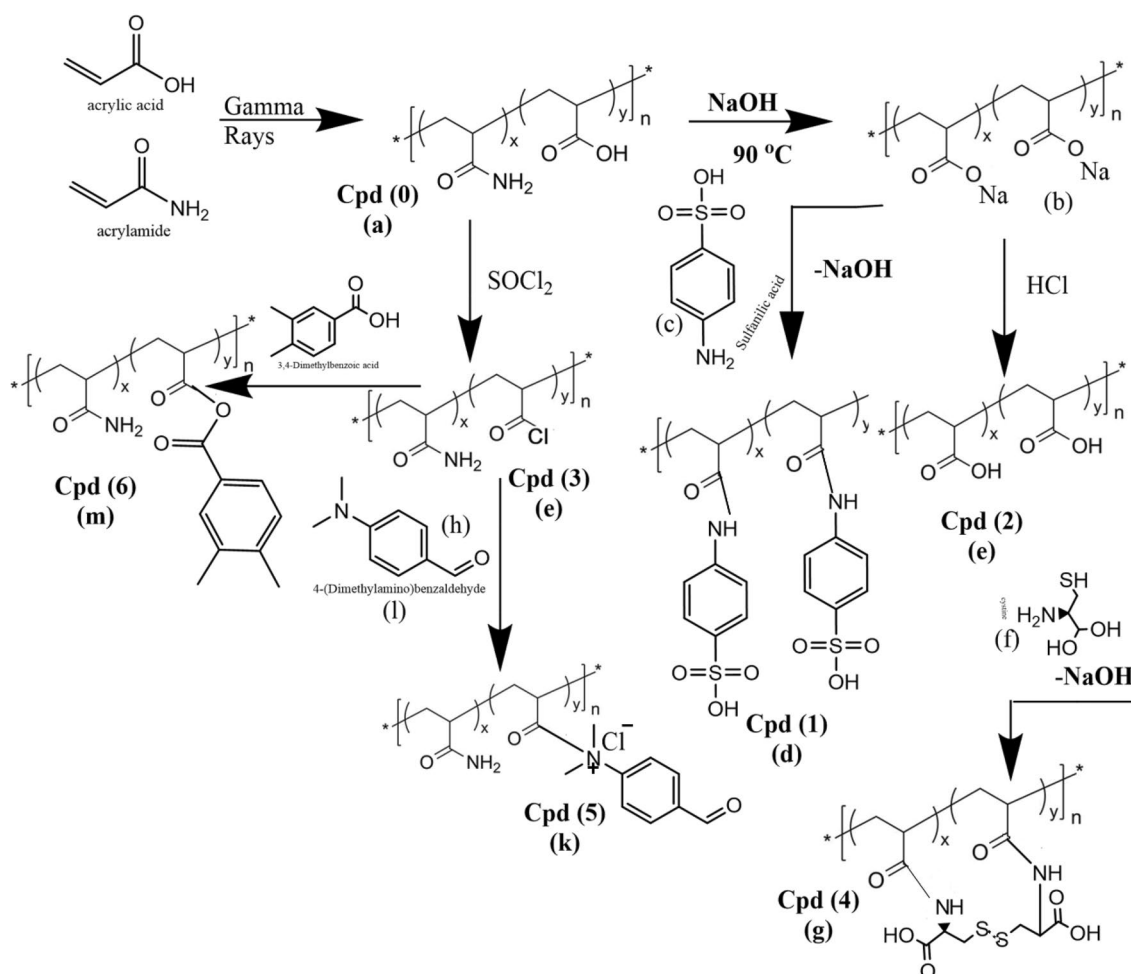


Figure 1. Chemical modification of p(AAm-co-AAc) hydrogel.

sample is thoroughly mixed with the sulfanilic acid. The reaction mixture is stirred for one hour at ambient temperature, then hydrothermally treated at 60 °C for three hours. The sulfanilic acid reacts with functional groups in the hydrogel, modifying the hydrogel by introducing new groups. At the end of the modification process, the modified p(AAm-co-AAc) hydrogel is filtered, then washed with ethanol and 0.1 M HCl solutions to remove unreacted sulfanilic acid or reaction byproducts. Finally, the hydrogel is washed with ethyl acetate to ensure the removal of residual solvents and impurities. The washed sample of sulfonated p(AAm-co-AAc) hydrogel (coded as Cpd1) is dried at 50 °C, and then stored in a closed glass bottle for further use.

Reaction with sodium hydroxide

A certain weight of p(AAm-co-AAc) hydrogel sample (Cpd 0) was allowed to swell in water, then heated at 90 °C in NaOH (0.5 M) solution, followed by the reaction with 1 M HCl to give Cpd (2), as shown in Fig. 1. The approach involves alkaline hydrolysis of the amino (–NH₂) groups in the Cpd 0 sample and conversion into carboxyl (–COOH) groups, followed by a reaction with HCl to obtain the modified hydrogel (Cpd 2).

Reaction with thionyl chloride

In a three-neck flask, a known weight of the bare p(AAm-co-AAc) hydrogel (Cpd 0, 0.5 g) is added to thionyl chloride (SOCl₂, 2 mol) solution prepared in methylene chloride solvent. The hydrogel and SOCl₂ solution mixture is stirred under the conditions (80 °C for 7 h). Thermal treatment facilitates the response among the hydrogel and SOCl₂, leading to the desired modification. After the specified reaction (t), ice crystals are added to quench any unreacted SOCl₂ and prevent further reaction. Then, the obtained modified p(AAm-co-AAc) hydrogel (Cpd 3; Fig. 1) is filtered and washed with methylene chloride solvent to remove any residual reactants or byproducts. Subsequently, the hydrogel is dried in an oven at 50 °C (24 h) and then stored in a closed glass container till further use.

Reaction with cystine

An aqueous solution of 0.8 mol of cystine (100 mL) is freshly prepared and added slowly to the Cpd 0 hydrogel (0.5 g) under stirring to ensure uniform mixing. After the complete addition of the cystine solution, the mixture is allowed to stand overnight. The mixture is then allowed for thermal soxhtelation under stirring at 50 °C for 60 min to facilitate the reaction process between cysteine and hydrogel. After the thermal treatment, the solid product of the modified p(AAm-co-AAc) hydrogel (termed Cpd 4, Fig. 1) is filtered off from the reaction mixture and then dried to remove any remaining moisture and solvents.

Reaction with 4-(Dimethylamino)benzaldehyde

A solution of 0.2 mol of 4-(Dimethylamino)benzaldehyde is prepared in 100 mL tetrahydrofuran (THF). The prepared 4-(Dimethylamino)benzaldehyde solution is added drop-wise to the modified p(AAm-co-AAc) hydrogel (Cpd 3, 0.5 g) with stirring to ensure proper mixing and distribution of the solution. After adding the 4-(Dimethylamino)benzaldehyde solution, the mixture can stand at ambient temperature for 24 h, followed by soxhtelation at 65 °C for six hours. The elevated temperature and stirring help facilitate the desired modification reaction by the promoted interaction between the hydrogel and 4-(Dimethylamino)benzaldehyde. After the reaction, the obtained solid product is thoroughly washed with ethanol and water to remove any residual reactants or byproducts. The washed solid of the modified p(AAm-co-AAc) hydrogel is then dried to remove any remaining moisture and labeled as Cpd 5, according to Fig. 1.

Reaction with 3,4-Dimethylbenzoic acid

A 0.25 mol of 3,4-Dimethylbenzoic acid solution is prepared in 100 mL of acetonitrile and mixed with the Cpd 3 hydrogel sample (0.5 g) under stirring for seven hours. After the mixing step, the mixture is heated to 60 °C under stirring for six hours to promote the reaction of 3,4-Dimethylbenzoic acid with the hydrogel. After the reaction, the solid sample obtained is separated by filtration and washed with ethanol to purify the modified hydrogel. The washed solid sample is finally dried to remove any remaining moisture and labeled as Cpd 6, according to Fig. 1.

Characterization

Attenuated total reflectance-Fourier transform infrared (ATR-FTIR) spectroscopy and scanning electron microscopy (SEM) characterization techniques were employed to evaluate the surface functionality and structural changes of the p(AAm-co-AAc) hydrogel before and after chemical modification strategies. ATR-FTIR spectroscopy was performed using a Vertex 70 FTIR spectrometer equipped with a HYPERION™ series microscope from Bruker Optik GmbH, Germany. ATR-FTIR spectroscopy is a powerful technique for providing information on the modified hydrogels' surface functionality and chemical structure. The OPUS 6.0 software from BRUKER was used for data processing, including baseline correction using the rubber band method with CO₂ bands excluded. The effect of chemical modification methods on the morphological features and structural characteristics of p(AAm-co-AAc) hydrogel were also evaluated using an SEM microscope (model Zeiss-EVO, MA-10, variable UK).

Adsorption study

This study uses a synthetic water solution with 1000 mg/L salinity (as NaCl) and a mixture of HM cations (e.g., Cu²⁺, Ba²⁺, and Sr²⁺ ions) to simulate the actual composition of natural surface water bodies. For the adsorption process, the adsorption affinity of modified p(AAm-co-AAc) hydrogels for the three HM ions (Cu²⁺, Ba²⁺, and Sr²⁺) from their water solutions were conducted in batch mode under fixed operating conditions (2 g/L adsorbent

mass, agitation speed of 150 rpm, and solution pH 6.5 ± 0.3). At different (t) intervals (1–24 h), the effluent water sample (5 mL) was withdrawn, then filtered and subjected to analysis using Ion-chromatography (IC Dionex DX-600, USA) and atomic absorption spectroscopy (AAS: Analytik Jena Zenit 700p, Germany) to quantify the residual concentration of HM ions in the treated water samples. The adsorption affinity of hydrogels (bare and modified) for the three HM cations was also investigated and compared in relation to the effects of adsorption time (1–24 h), initial HM ions' concentrations (Cu^{2+} : 1–50 mg/L; Ba^{2+} : 10–100 mg/L; Sr^{2+} : 10–100 mg/L), and solution temperature (15–45 °C). These comprehensive studies aimed to get a deeper insight into the adsorption mechanism based on kinetic, isotherm, and thermodynamic analyses. Exact repeatability for each experimental run was also tested to calculate the systematic error during adsorption. The adsorption performance of tested hydrogel adsorbents for HM uptake from water solution was evaluated by different metrics like adsorption efficiency (RE (%), Eq. (1)) and capacity of adsorption (Q_t (mg/g), Eq. (2)).

$$RE(\%) = \frac{C_o - C_t}{C_o} \times 100 \quad (1)$$

$$Q_t = \frac{C_o - C_t}{m} \times V. \quad (2)$$

Here, C_o and C_t (mg/L) are the initial concentration and residual concentration of tested HM ions in water solution before and after the adsorption process, respectively, at different (t) intervals (t, h). The terms m (g) and V (L) refer to the hydrogel mass (gram) and solution volume (liter) used during the adsorption process, respectively.

Results and discussion

Characterization data

Effect of synthetic conditions on the swelling and gel fraction of p(AAm-co-AAc) hydrogel

Figure 2a shows the p(AAm-co-AAc) hydrogel materials swelling degree as a function of comonomer concentration (AAc and AAm) from 12 to 27 v/wt%. At a co-monomer concentration of 12 v/wt%, the hydrogel exhibited the highest swelling degree of 400% after 240 min. As the co-monomer concentration increased to 22 v/wt% and 27 v/wt%, the swelling degree decreased to 240% and 200%, respectively. This reduction in the swelling capacity could be ascribed to the impact of higher co-monomer concentrations on crosslinking density, the hydrophilic nature of hydrogel, and the polymer network structure that played a key role in determining the swelling behavior of hydrogels. For the gel fraction in Fig. 2b, it was denoted that the p(AAm-co-AAc) hydrogel had the highest gel fraction at 27 v/wt % co-monomer concentration level. A higher gel fraction suggests higher crosslinking and a more stable and structurally robust hydrogel. Compared to hydrogels with higher polyacrylamide content in Fig. 2c, the lower swelling degrees of p(AAm-co-AAc) hydrogels at higher acrylic acid content could also attributed to intermolecular hydrogen bonds formed by acrylic acid carboxyl groups (-COOH). These intermolecular hydrogen bonds restrict the uptake of water molecules by the hydrogel, leading to a decrease in swelling capacity. In contrast, hydrogels with higher polyacrylamide content are expected to have a higher swelling degree due to the absence of carboxyl groups and the resulting lower propensity for hydrogen bond formation. Figure 2d shows that the gel fraction of the p(AAm-co-AAc) hydrogel increases as the acrylic acid content decreases. The gel fraction measures the extent of crosslinking within the hydrogel network. A higher gel fraction suggests higher crosslinking and a more stable and structurally robust hydrogel. The impact of gamma irradiation dose (10–30 kGy) on the degree of swelling and gel fraction of p(AAm-co-AAc) (25:75) hydrogel samples was studied, and the results are shown in Fig. 2e,f. As can be observed in Fig. 2e and f, the p(AAm-co-AAc) (25:75) hydrogel samples demonstrated a decrease in the swelling degree and an increase in the gel fraction as gamma irradiation doses rose from 10 to 30 kGy. Gamma irradiation generates free radicals within the hydrogel matrix to initiate crosslinking reactions among the polymer chains, resulting in a denser network structure at a higher irradiation dose. This denser network restricts the uptake of water molecules, leading to a decrease in the degree of swelling.

Surface functionalities of p(AAm-co-AAc) hydrogels

Figure 3 shows the FT-IR spectra of all poly(acrylic acid-co-acrylamide) hydrogels (Cpd x, where x = 0 to 6) before and after modification strategies. The FTIR spectrum of the unmodified hydrogel (Cpd 0; Fig. 3a) showed absorption peaks at around 3656 cm^{-1} and 3531 cm^{-1} , assigned to the stretching vibrations of the -OH groups in the hydrogel structure from AAc and AAm monomers, respectively. Two peaks at 2976 cm^{-1} and 2855 cm^{-1} are also observed, corresponding to the asymmetric and symmetric stretching vibrations of the -CH₂- groups. The peak at 1450 cm^{-1} is assigned to the bending vibration of the -OH hydroxyl groups. The peaks at 1059 cm^{-1} and 827 cm^{-1} are attributed to the stretching vibrations of the C-O and C-C bonds, respectively. The absorption peaks at 1685 cm^{-1} and 1756 cm^{-1} are also ascribed to the C=O stretching vibrations in the amide and carboxyl groups, respectively. For the FTIR spectrum of modified Cpd1 hydrogel (Fig. 3b), different FTIR peaks are recorded as follows: 1450 cm^{-1} (C-N stretching in benzenoid rings), 612 cm^{-1} (the stretching vibrations of C-S bonds), and 694 cm^{-1} (bending vibration of SO₃ groups). These peaks suggest the existence of sulfonate functional groups in the modified Cpd1 hydrogel. In Fig. 3c, the characteristic FTIR peak of C=O is observed as a very broad peak at 1660 cm^{-1} , indicating that the carboxylic groups in the Cpd2 hydrogel have increased compared to the blank Cpd0 sample. The existence of carboxylic groups can be attributed to the modification approach or the introduction of functional groups like acrylic acid during the synthesis. Carboxylic groups are known for their ability to form hydrogen bonds and exhibit acidic properties. They can contribute to the adsorption capacity and selectivity of the hydrogel toward specific ions or molecules³⁰.

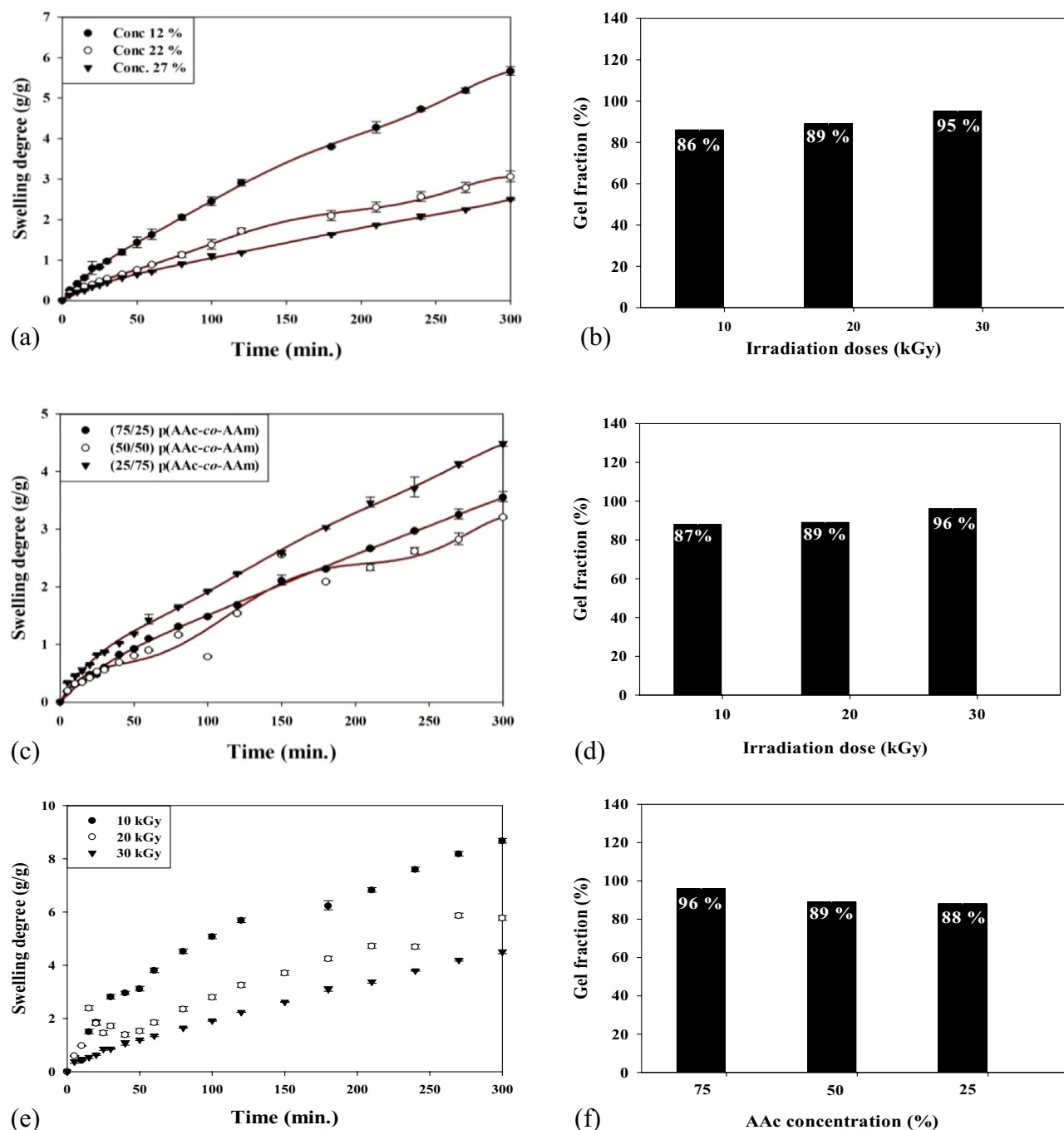


Figure 2. Effect of comonomer concentration and gamma irradiation on the swelling degree and gel fraction of p(AAm-co-AAc) hydrogel.

(Fig. 3d) also shows a new characteristic peak at $1830\text{--}1751\text{ cm}^{-1}$ related to the stretching vibration of the acyl chloride (-COCl) group after the reaction of hydrogel with thionyl chloride (SOCl_2). The acyl chloride functional group (-COCl) is highly reactive and can participate in various chemical reactions. The acyl chloride group can be a reactive site for further functionalization or chemical reactions. It can be utilized to introduce specific functional groups or linkers that enhance the adsorption properties or enable targeted interactions of the hydrogel with specific ions, molecules, or substances³¹. For instance, a new absorption peak at 1729 cm^{-1} is observed in the FTIR spectrum of Cpd4 hydrogel (Fig. 3e), attributing to a carbonyl stretch vibration of (C=O) groups³². Further changes were observed in the broad FTIR peaks around 3735 cm^{-1} and 3630 cm^{-1} for -OH and -NH_2 groups, respectively. A new FTIR peak of the SH bend is also located around 949 cm^{-1} ³³. The FTIR spectrum of the Cpd5 (Fig. 3f) presents two characteristic related to the presence of 4-amino benzaldehyde at 2790 and 2659 cm^{-1} for the H-C=O stretching vibration of carbonyl-containing functionality and aldehydic C-H stretching vibration, respectively. In Fig. 3g, the FTIR analysis of Cpd6 hydrogel also displays the stretching

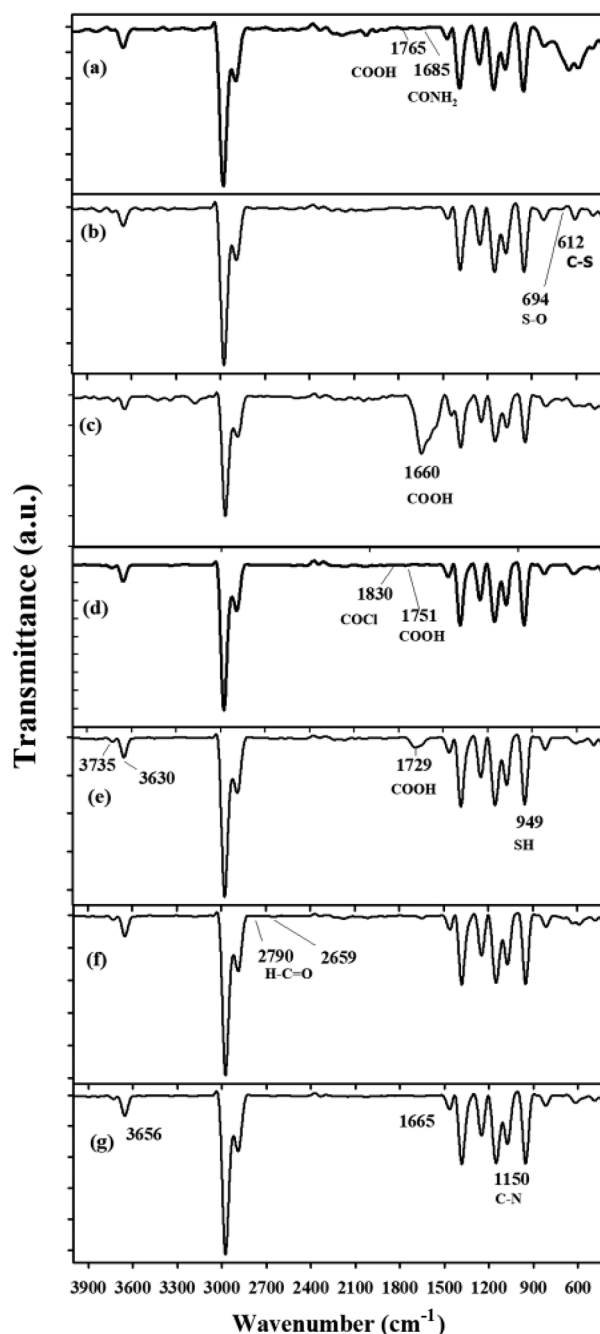


Figure 3. The FTIR spectra of bare and chemically modified p(AAm-co-AAc) hydrogels: (a) Cpd (0), (b) Cpd (1), (c) Cpd (2), (d) Cpd (3), (e) Cpd (4), (f) Cpd (5), and (g) Cpd (6).

vibration peaks of O–H and C=O groups at 3656 cm^{-1} and 1665 cm^{-1} , respectively. The FTIR peak at 1150 cm^{-1} is also assigned to the aromatic C–N stretching, possibly originating from 4-aminobenzoic acid or other aromatic moieties introduced during the modification approach³⁴. These peaks suggest incorporating 4-aminobenzoic acid, which contains hydroxyl and carboxylic acid functional groups, into the modified hydrogel. Introducing these functional groups can enhance the hydrogel's interactions with target metal ions or molecules, providing specific adsorption or binding capabilities. The above FTIR spectra confirm the polymeric chains' microstructural configuration and chemical modifications.

Morphological features of p(AAm-co-AAc) hydrogels

The microstructure and surface morphology of the bare and modified hydrogel samples using SEM analysis are shown in Fig. 4. The SEM images confirm that all modified p(AAm-co-AAc) hydrogels (Cpd 1 - Cpd6) retain porous and interconnected structures similar to the bare hydrogel sample (Cpd0). This suggests that the chemical

modification approaches did not significantly alter the crosslinking structure of Cpd0 hydrogel. In particular, the Cpd0 exhibited a smooth interface with uniformly distributed open pores. These inherent porous structures are slightly altered after chemical modification processes, confirming the successful deposition of the chemical functional groups within the prepared hydrogels. For example, the modified cpd1 hydrogel with sulfanilic acid ($-\text{SO}_3\text{H}$) groups showed a higher swelling property and larger pore diameter than bare Cpd0. This is attributed to the hydrophilic nature of the sulfonate groups, which promote water absorption and swelling of the hydrogel. Compared to Cpd0, the modified Cpd4 hydrogel with cysteine functionality showed smaller pore diameters with higher agglomerates of polymer chains. Such observation was ascribed to the formation of intramolecular hydrogen bonds among the hydroxyl (OH), thiol (SH), and amino (NH_2) groups, resulting in a denser network structure. In contrast, hydrogels with weaker intramolecular hydrogen bonding, like Cpd2, Cpd3, Cpd5, and Cpd6, showed larger pore sizes with a lower aggregation of polymer chains.

Adsorption applicability of (AAm-co-AAc) hydrogels for Cu^{2+} , Ba^{2+} , and Sr^{2+} ions

Herein, the adsorption efficiency of blank and modified p(AAm-co-AAc) hydrogels for the three HMs (Cu^{2+} , Ba^{2+} , and Sr^{2+} ions) was assessed based on adsorption isotherm, adsorption kinetic, and thermodynamic analyses.

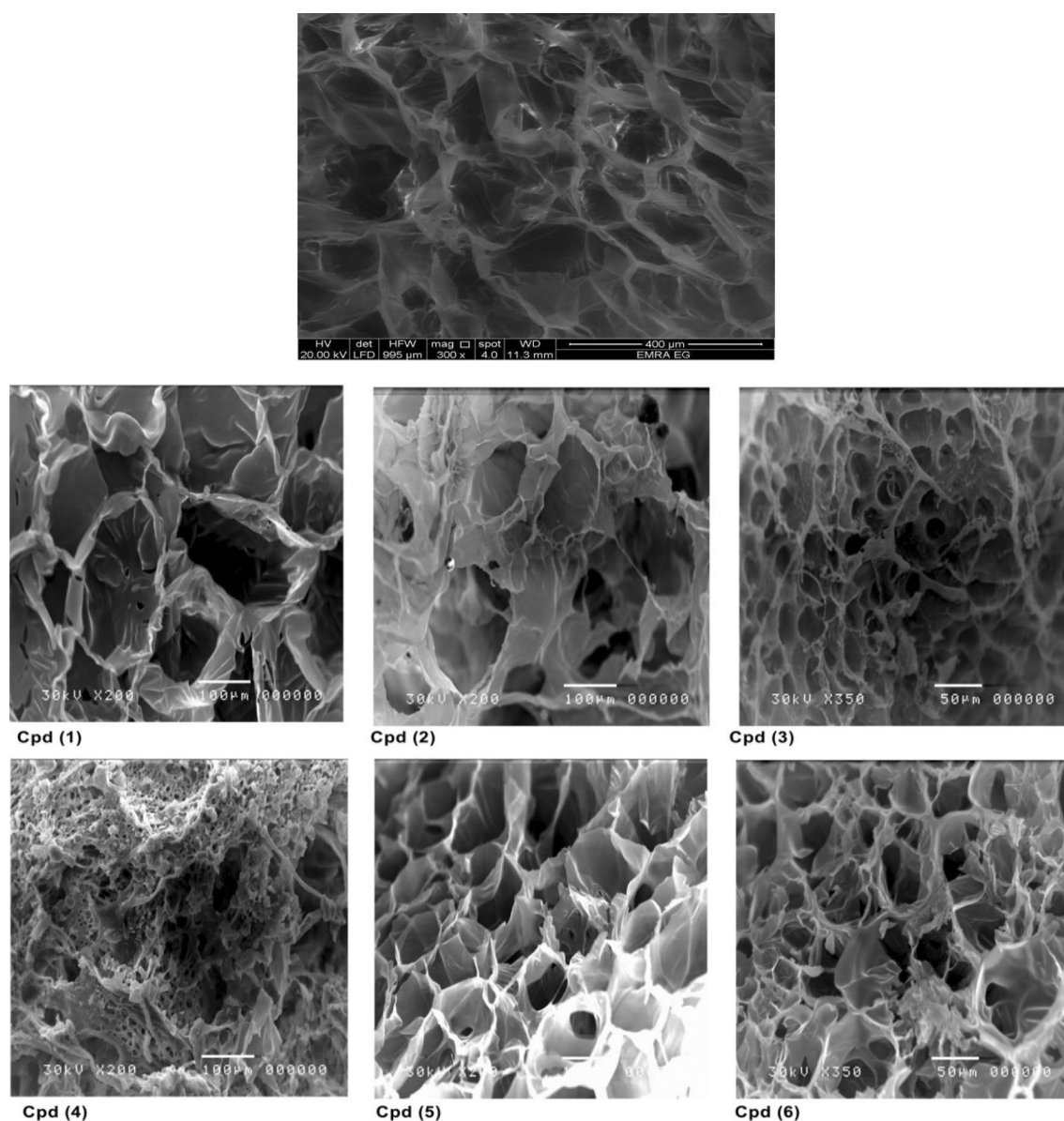


Figure 4. SEM images of unmodified p(AAm-co-AAc) hydrogel (Cpd0) and their modified forms (Cpd1 – Cpd6).

Effect of initial HM ion concentrations: adsorption isotherm modeling

Figure 5 presents the adsorption capacity of the blank and modified p(AAm-co-AAc) hydrogel adsorbents for the three HM ions (Cu^{2+} , Ba^{2+} , and Sr^{2+}) as a function of their varying initial concentrations. As can be seen, the adsorption capacities of all tested hydrogel adsorbents increased linearly with the initial concentration of the HM ions. Besides, all modified hydrogel samples demonstrated a higher adsorption affinity for the three HM ions than the blank sample (Cpd0). Among the modified hydrogels, the Cpd2 hydrogel adjusted with sodium hydroxide exhibited the highest affinity for the adsorption recovery of the three HM ions. Conversely, the modification strategy of hydrogel with thionyl chloride (Cpd3) significantly reduced the adsorption capability for Cu^{2+} ion removal (Fig. 5a). In comparison, the chemically modified Cpd6 hydrogel exhibited a slightly lower adsorption uptake for Ba^{2+} and Sr^{2+} ions compared to all other modified hydrogels (Fig. 5b,c).

For Cu^{2+} ion removal (Fig. 5a), the adsorption capacity of the hydrogels ranked as $\text{Cpd2} > \text{Cpd5} > \text{Cpd1} > \text{Cpd6} > \text{Cpd4} > \text{Cpd0} > \text{Cpd3}$. Specifically, the adsorption capacity of Cu^{2+} onto Cpd2 hydrogel was 2.3-fold higher than the unmodified Cpd0 hydrogel. As the initial Cu^{2+} ion concentration increased from 1 to 50 mg/L, the adsorption capacity of Cu^{2+} onto Cpd2 linearly increased from 0.50 to 13.66 mg/g, respectively. Similarly, in Fig. 5b, all modified hydrogel samples demonstrated high adsorption affinity for Ba^{2+} ions (100 mg/L) compared to the Cpd0, showing the maximum capacity rank order of $\text{Cpd2} (36.4 \text{ mg/g}) > \text{Cpd6} (34.9 \text{ mg/g}) \geq \text{Cpd1} (34.5 \text{ mg/g}) \geq \text{Cpd3} (33.9 \text{ mg/g}) \geq \text{Cpd4} (33.4 \text{ mg/g}) > \text{Cpd5} (25.5 \text{ mg/g}) > \text{Cpd0} (23.6 \text{ mg/g})$. Comparatively, in the case of Sr^{2+} ions (Fig. 5c), only Cpd1 and Cpd2 hydrogels exhibited a higher adsorption capacity for Sr^{2+} ions than the blank hydrogel (Cpd0) by 1.23 to 1.44 times of magnitude, respectively. All other modified hydrogels (e.g., thionyl chloride, cysteine, 4-(Dimethylamino) benzaldehyde, or 3,4-Dimethylbenzoic acid) showed a decline in the adsorption affinity for Sr^{2+} ion uptake compared to the unmodified Cpd0 adsorbent. The adsorption capacities of $\text{Ba}^{2+}/\text{Sr}^{2+}$ ions onto Cpd2 were also increased from 4.9/3.36 mg/g to 36.4/27.31 mg/g as their initial concentration levels increased from 10 to 100 mg/L, respectively. Based on the maximum adsorption capacity, the adsorption selectivity of Cpd2 (as the best performer adsorbent) for the three HM ions can be ranked as $\text{Ba}^{2+} (36.4 \text{ mg/g}) > \text{Sr}^{2+} (27.31 \text{ mg/g}) > \text{Cu}^{2+} (13.7 \text{ mg/g})$ (Fig. 5a–c). These results demonstrated the effectiveness of the alkaline (NaOH) hydrolysis method in improving the adsorption property of the p(AAm-co-AAc) hydrogel for

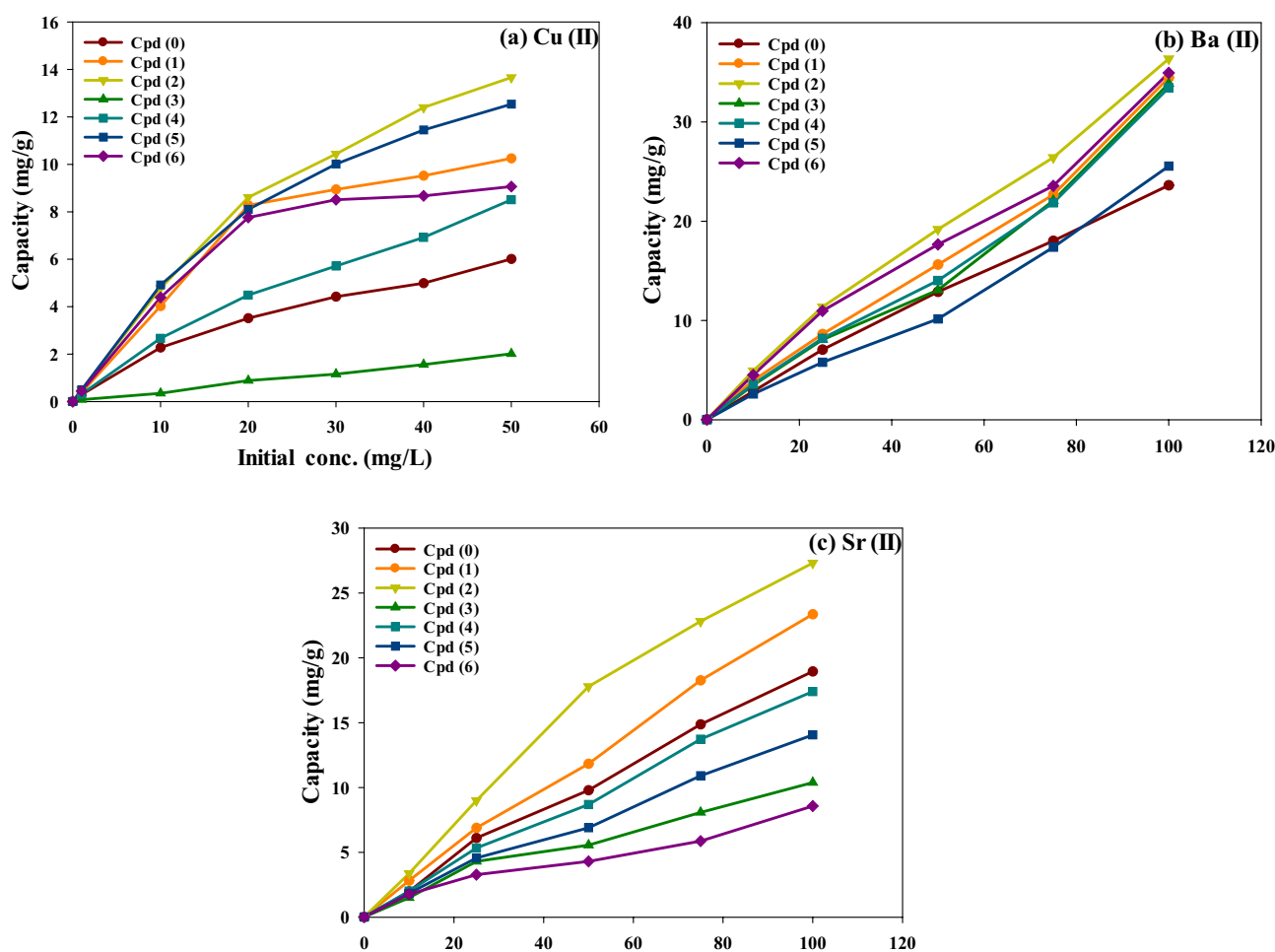


Figure 5. The adsorption capacity of blank and modified p(AAm-co-AAc) hydrogels towards varying initial concentrations of (a) Cu^{2+} , (b) Ba^{2+} , and (c) Sr^{2+} ions from synthetic water solution at 1000 mg/L salinity and 25 °C.

Cu^{2+} , Ba^{2+} , and Sr^{2+} ions from the salty water solution. The choice of modifying agent and the specific HM ion being targeted also played a crucial role in determining the adsorption performance of the hydrogel adsorbents.

Based on the above adsorption data, three adsorption isotherm models were employed to describe the effect of hydrogel surface functionalities on the adsorption mechanism of the adsorbate ions in an aqueous solution. Using nonlinear regression analysis, this work utilized Freundlich (Eq. (3)), Langmuir (Eq. (4)), and Tempkin (Eq. (5)) isotherm models to analyze the adsorption equilibrium mechanism of the three metal ion adsorbates by hydrogel adsorbents²². The Freundlich model is the earliest known empirical equation and is shown to be consistent with an exponential distribution of active centers characteristic of heterogeneous surfaces. The Langmuir equation validates monolayer adsorption onto the adsorbent surface with a finite number of identical sites. Tempkin isotherm considered the effects of indirect adsorbent/adsorbate interactions on adsorption, assuming that the heat of adsorption of all the molecules in the layer would decrease linearly with coverage due to adsorbent/adsorbate interactions³⁵. The comprehensive details outlining the theoretical hypothesis for the isotherm models can be found in the Supplementary Information.

$$q_e = K_f C_e^{1/n} \quad (3)$$

$$q_e = \frac{q_m K_L C_e}{1 + K_L C_e} \quad (4)$$

$$q_e = \frac{RT}{B_T} \ln A_T C_e \quad (5)$$

where q_e is the equilibrium capacity of adsorbed metal ions by the hydrogel (mg/g), q_m is the theoretical monolayer adsorption capacity (mg/g) at equilibrium, C_e (mg/L) is the equilibrium concentration of the adsorbate ions. K_f (L/g) is the Freundlich constant related to the adsorption capacity, whereas n_f refers to adsorption intensity. Langmuir constant, K_L , represents the adsorption equilibrium (L/mg). R is the universal gas constant (0.08314 kJ/mol K), and T is the adsorption temperature in Kelvin (K). Besides, B_T and A_T refer to adsorption energy (i.e., heat of adsorption: kJ/mol) and equilibrium binding constant (L/g), respectively.

According to the R^2 values in Table 1, the adsorption equilibrium data of the three metal ions onto all hydrogels demonstrated a good fit with the three isotherm models. Amongst, the Freundlich model best describes the adsorption behavior of the three HM ions onto blank and modified hydrogels, with fitting order of Freundlich ($R^2 = 0.90\text{--}0.992$), Langmuir ($R^2 = 0.77\text{--}0.991$), and Tempkin ($R^2 = 0.74\text{--}0.993$). The good-of-fit to the Langmuir and Freundlich models indicates that the adsorption mechanism of HM ions onto all modified hydrogels is a complex phenomenon and might follow both monolayer and multilayer adsorption mechanisms onto heterogeneous adsorbent surfaces (i.e., neglect indirect interactions). The multilayer adsorption phenomenon observed in the Freundlich model suggests that multiple sites are available for adsorption on the hydrogel surface, allowing for the formation of numerous adsorbate molecules²⁷. This behavior can be attributed to the hydrogel's porous structure and heterogeneous nature, which provides ample surface area and various binding sites for the adsorbate ions²².

From the isotherm constants in Table 1, both Cpd2 and Cpd5 hydrogels had the highest Freundlich constant ($K_f = 5.68\text{--}5.79$ L/g) for Cu^{2+} ions. Also, Cpd2 recorded the highest K_f value of 6.666 and 3.105 L/g for Ba^{2+} and Sr^{2+} adsorption, respectively. Based on the K_f values, the adsorption selectivity of Cpd2 for the three metal ions ranked as $\text{Ba}^{2+} > \text{Cu}^{2+} > \text{Sr}^{2+}$, agreeing with the experimental capacity order (Fig. 5). A more prominent Freundlich exponent ($n_f > 1$) also indicated more surface heterogeneity, resulting in a non-linearity adsorption isotherm. The higher surface heterogeneity is ascribed to multiple surface functional groups as verified by FTIR analysis earlier. It is also well known that the adsorption energy could provide crucial information about the strength of the adsorption interaction between metal ions and hydrogel surface functionalities. In this respect, the Tempkin B_T values in Table 1 represent the heat of adsorption. By considering the positive B_T values, the adsorption process of HM ions onto the hydrogel adsorbents could imply favorable endothermic adsorption. Analyzing the B_T data in Table 1, we can observe variations in the adsorption energies among the different samples and metal ions. In particular, the largest adsorption energy was observed in the presence of Cu^{2+} ions uptake, ranging from 1.20 kJ/mol (Cpd1) to 5.781 kJ/mol (Cpd3). Also, all modified hydrogel adsorbents need higher energy for Cu^{2+} adsorption than Sr^{2+} and Ba^{2+} ions. This explains the lower adsorption capacity of copper ions onto all modified hydrogels compared to barium and strontium ions from water solution. The adsorption energy of metal ions onto all hydrogel adsorbents ranked in the ascending order Ba^{2+} ($K_T = 0.25$ to 0.457 kJ/mol) $<$ Sr^{2+} ($K_T = 0.268$ to 1.074 kJ/mol) $<$ Cu^{2+} ($K_T = 1.20$ to 5.781 kJ/mol). The lower adsorption energy of Ba^{2+} explains the reasons for the favorable Ba^{2+} uptake by blank and modified hydrogels. In this case, it is assumed that the adsorption process of Ba^{2+} ions obeyed mainly a physical adsorption mechanism (weak interaction) and can be spontaneously stimulated via relatively weaker chelating bonds under normal operating conditions. In contrast, the more considerable adsorption energies for Cu^{2+} ions declared that higher heat energy is needed to induce the chemical interaction between hydrogel surface functionalities with Cu^{2+} ions. Overall, the estimated Tempkin K_T values (adsorption energy constants) in Table 1 suggested that there is a significant variation in the specific interaction mechanisms among the metal ions and the hydrogel adsorbents due to the differences in the composition and structure of the p(AAm-co-AAc) hydrogel samples.

Effect of adsorption time: kinetic modeling

Figure 6 shows the adsorption removal of three metal ions (10 mg/L Cu^{2+} , 50 mg/L Ba^{2+} , and 50 mg/L Sr^{2+}) from a solution mixture onto all prepared p(AAm-co-AAc) hydrogel adsorbents as a function of adsorption time. As

Hydrogels/Constants	Metal adsorbates								
	Cu ²⁺			Ba ²⁺			Sr ²⁺		
(a)	Freundlich model								
	K _F	n _f	R ²	K _F	n _f	R ²	K _F	n _f	R ²
Cpd (0)	0.906	1.941	0.992	1.003	1.259	0.998	0.596	1.193	0.988
Cpd (1)	3.871	3.253	0.909	0.931	0.999	0.900	0.798	1.177	0.994
Cpd (2)	5.683	3.488	0.976	6.666	2.084	0.941	3.105	1.719	0.947
Cpd (3)	0.045	1.008	0.99	0.025	0.492	0.907	0.483	1.438	0.969
Cpd (4)	1.018	1.669	0.993	0.386	0.816	0.918	0.457	1.147	0.991
Cpd (5)	5.793	4.139	0.969	0.085	0.688	0.963	0.372	1.181	0.986
Cpd (6)	4.076	3.894	0.918	4.592	1.831	0.907	0.384	1.463	0.939
(b)	Langmuir model								
	q _m	K _L	R ²	q _m	K _L	R ²	q _m	K _L	R ²
Cpd (0)	8.104	0.061	0.986	7.246	0.091	0.996	73.58	0.006	0.987
Cpd (1)	10.894	0.452	0.937	3.74	4.46	0.89	106.721	0.005	0.991
Cpd (2)	13.057	0.916	0.961	49.507	0.069	0.875	41.82	0.042	0.981
Cpd (3)	25.653	0.051	0.991	3.16	1.33	0.9	21.663	0.011	0.956
Cpd (4)	13.651	0.043	0.985	6.27	1.76	0.77	91.875	0.004	0.989
Cpd (5)	10.922	3.798	0.917	6.43	0.00715	0.931	69.196	0.003	0.981
Cpd (6)	9.455	0.757	0.992	43.68	0.065	0.843	19.953	0.008	0.904
(c)	Temppkin model								
	B _T	A _T	R ²	B _T	A _T	R ²	B _T	A _T	R ²
Cpd (0)	2.097	2.195	0.934	0.311	0.267	0.943	0.359	0.193	0.945
Cpd (1)	1.200	5.901	0.922	0.266	0.506	0.758	0.315	0.258	0.914
Cpd (2)	1.349	46.815	0.979	0.457	7.543	0.821	0.268	0.421	0.993
Cpd (3)	5.781	0.781	0.744	0.250	0.349	0.688	0.744	0.205	0.93
Cpd (4)	1.480	2.103	0.896	0.254	0.373	0.74	0.401	0.188	0.921
Cpd (5)	1.707	133.304	0.983	0.289	0.202	0.772	0.525	0.19	0.903
Cpd (6)	1.557	13.74	0.961	0.343	1.523	0.836	1.074	0.257	0.838

Table 1. Adsorption isotherm model constants of three metal ions adsorbed by blank and modified p(AAm-co-AAc) hydrogel adsorbents.

can be seen, there is a linear increment in the removal efficiency of the three ions during the first two hours by all modified hydrogel adsorbents, suggesting their fast initial uptake rates of metal ions. Specifically, all modified p(AAm-co-AAc) hydrogels exhibited a quicker removal rate for Cu²⁺ and Ba²⁺ ions than the blank Cpd0, approaching the equilibrium state after approximately 10 h. On the other hand, the equilibrium time of Sr²⁺ ion onto all hydrogels reached after around 18 h. This verifies the synergistic impact of exchangeable functional groups on the enhanced metal adsorption rate. Besides, the adsorption of Sr²⁺ ions onto the hydrogel adsorbents is slower than Cu²⁺ and Ba²⁺ ions. In particular, Cpd2 outperformed all other hydrogels for the adsorption removal of the three metal ions, following the order of Ba²⁺ (Q_e = 19.18 mg/g) > Sr²⁺ (Q_e = 17.79 mg/g) > Cu²⁺ (Q_e = 4.78 mg/g).

Three kinetic models were applied to further investigate the obtained adsorption data, including nonlinear Lagergren's pseudo-first-order (Eq. (6)), pseudo-second-order (Eq. (7)), and Elovich's (Eq. (8)) kinetic models³⁶. The comprehensive details outlining the theoretical hypothesis for the kinetic models can be found in the Supplementary Information.

$$q_t = q_e(1 - e^{-K_1 t}) \quad (6)$$

$$q_t = \frac{q_e^2 K_2 t}{1 + q_e K_2 t} \quad (7)$$

$$q_t = \frac{1}{\beta} \ln(1 + \beta \alpha t) \quad (8)$$

where, q_e (mg/g) and q_t (mg/g) are the ions adsorbed at equilibrium and time (t), respectively. k₁ (h⁻¹) and k₂ (g/mg.h) are the pseudo-first and pseudo-second rate constants, respectively. For Elovich model, α and β are the initial adsorption rate (mg/g.h) and desorption rate (g/mg) constants, respectively.

From the kinetic rate constants and fitting data (R² values) in Table 2, it can be noted that the kinetic data of all metal ions onto the blank and modified hydrogels fitted well with a pseudo-first-order model (R² > 0.951), followed by the pseudo-second-order model (R² > 0.927) and Elovich model (R² > 0.901). The high fitting adequacy

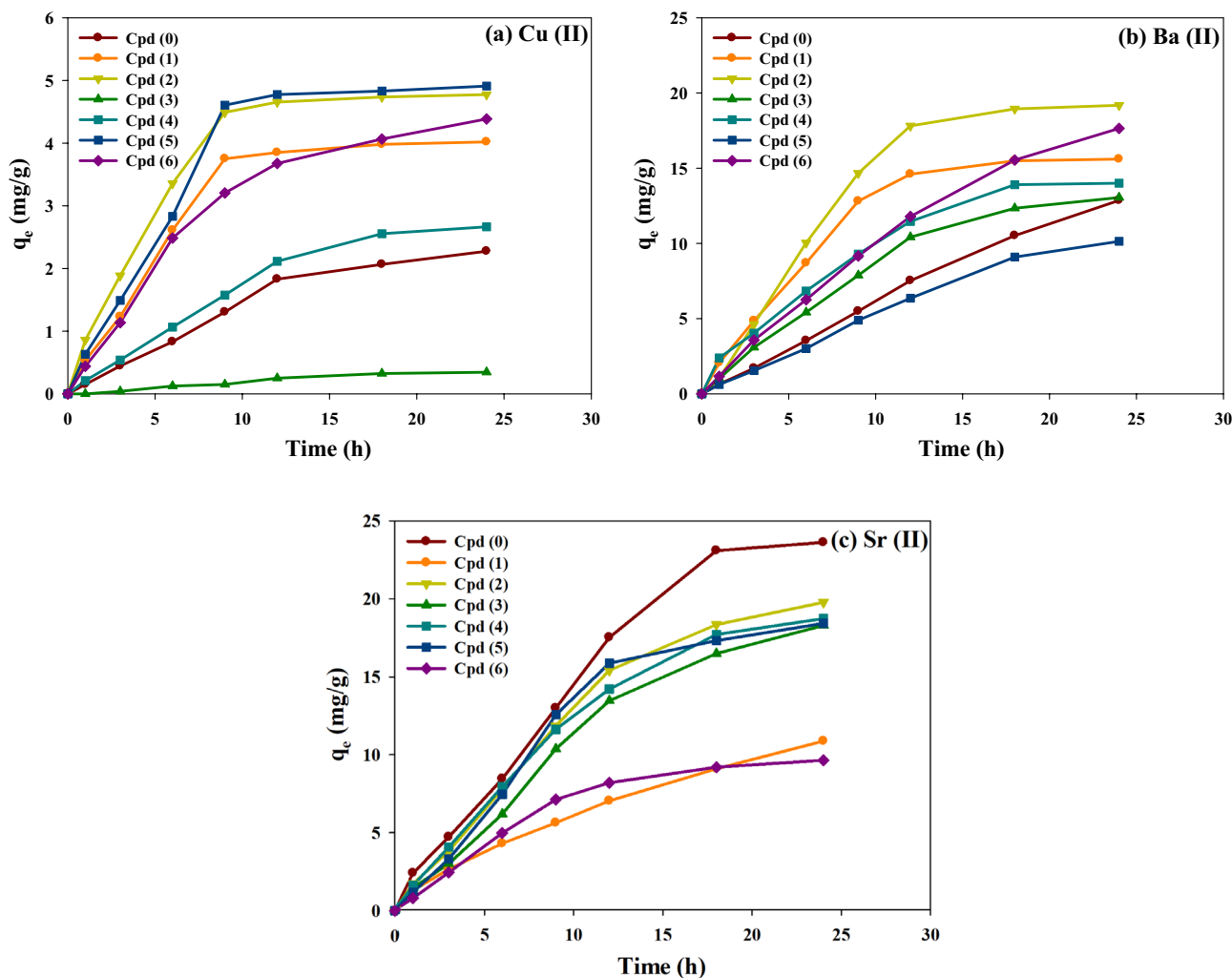


Figure 6. The correlation between adsorption time and adsorption capacity of three metal ions by modified and blank p(AAm-co-AAc) hydrogels.

of pseudo-first-order kinetic suggests that the physical adsorption (weak chemical adsorption and diffusion mechanisms) is the dominant rate-limiting step in the adsorption approach of the three metal ions onto the modified hydrogel adsorbents. Besides, the adsorption process could involve a rapid surface adsorption step, followed by slower mass transfer or diffusion processes at the equilibrium stage. Among the hydrogel samples, Cpd2 demonstrated the highest k_1 values for Cu^{2+} (0.194 h^{-1}) and Sr^{2+} (0.111 h^{-1}), whereas Cpd1 was superior for the enhanced adsorption kinetic of Ba^{2+} (0.137 h^{-1}). Comparatively, the lowest adsorption kinetic rates for metal ions were observed by Cpd0 for Ba^{2+} ions ($k_1 = 0.0019 \text{ h}^{-1}$) and Cpd3 for Cu^{2+} ($k_1 = 0.037 \text{ h}^{-1}$) and Sr^{2+} ($k_1 = 0.0055 \text{ h}^{-1}$).

Based on the Pseudo-second rate constants (k_2 values) in Table 2, the kinetic adsorption rate of metal ions can be ranked as: (i) Cpd2 > Cpd1 > Cpd3 \geq Cpd5 > Cpd6 > Cpd0 = Cpd1 for Cu^{2+} ion, (ii) Cpd1 > Cpd4 > Cpd2 > Cpd3 > Cpd5 > Cpd6 > Cpd0 for Ba^{2+} ion, and (iii) Cpd5 > Cpd6 > Cpd1 = Cpd2 = Cpd3 = Cpd4 > Cpd0 for Sr^{2+} ion. These data verified that the adsorption affinity of hydrogels for metal ions depends on both surface functionalities and the type of metal ions. From the Elovich model, the parameter α (mg/g.h) represents the number of ions adsorbed when the natural logarithm of (t)(ln t) is equal to zero, which corresponds to the adsorption quantity at the initial (t)(t = 1 h). Besides, the β values refer to the availability of adsorption sites on the prepared hydrogels for metal ions capture. By analyzing the importance of β and α , it is possible to understand the hydrogel's adsorption behavior and capacity for the studied metal ions. From Table 2, Cpd2 hydrogel demonstrated the highest β and α values of Cu^{2+} (2.141 g/mg and 1.704 mg/g.h, respectively), indicating its higher affinity for Cu^{2+} ions uptake compared with other chemically modified hydrogels. Besides, Cpd1 and Cpd0 recorded the maximum and minimum values of β for Ba^{2+} ions adsorption, recoding 0.148 and 0.033 g/mg, respectively. However, Cpd1 had the maximum α value of 3.284 mg/g.h for Ba^{2+} ions. Regarding Sr^{2+} adsorption, Cpd6 and Cpd2 recorded the highest β and α values of 0.265 g/mg and 0.1315 mg/g.h, respectively. These variations in β and α values for six Cpd x ($x = 1$ to 6) samples can be ascribed to the influence of the adsorbent functionalities, the nature of the metal ions, and the experimental conditions on the adsorption process. For example, certain functional groups may exhibit stronger interactions with specific metal ions, resulting in higher adsorption capacities. The pore

Adsorbates	Cu ²⁺			Ba ²⁺			Sr ²⁺		
(a)	Pseudo-first-order kinetic								
Hydrogels/Constants	q _e	k ₁	R ²	q _e	k ₁	R ²	q _e	k ₁	R ²
Cpd (0)	2.943	0.066	0.981	36.091	0.019	0.997	13.154	0.063	0.983
Cpd (1)	4.291	0.163	0.962	16.9	0.137	0.981	14.563	0.081	0.967
Cpd (2)	4.986	0.194	0.98	21.648	0.113	0.971	19.476	0.111	0.995
Cpd (3)	0.614	0.037	0.968	15.948	0.078	0.99	7.63	0.055	0.994
Cpd (4)	3.404	0.071	0.986	15.803	0.102	0.987	10.799	0.068	0.999
Cpd (5)	5.298	0.153	0.951	19.536	0.032	0.992	7.842	0.097	0.987
Cpd (6)	4.68	0.12	0.991	25.659	0.05	0.998	5.965	0.057	0.994
(b)	Pseudo-second-order kinetic								
Hydrogels/Constants	q _e	k ₂	R ²	q _e	k ₂	R ²	q _e	k ₂	R ²
Cpd (0)	4.597	0.010	0.977	66.627	0.0002	0.997	20.796	0.002	0.98
Cpd (1)	5.577	0.027	0.937	22.555	0.0050	0.966	22.093	0.003	0.96
Cpd (2)	6.221	0.031	0.954	30.461	0.0030	0.957	26.927	0.003	0.989
Cpd (3)	1.073	0.020	0.966	23.918	0.0020	0.986	11.993	0.003	0.993
Cpd (4)	5.236	0.009	0.982	22	0.0040	0.984	16.44	0.003	0.998
Cpd (5)	6.977	0.019	0.927	34.295	0.0010	0.991	11.304	0.006	0.98
Cpd (6)	6.417	0.015	0.983	41.499	0.0008	0.997	9.587	0.004	0.993
(c)	Elovich kinetic								
Hydrogels/Constants	α	β	R ²	α	β	R ²	α	β	R ²
Cpd (0)	0.214	0.573	0.973	0.679	0.033	0.997	0.896	0.125	0.976
Cpd (1)	1.045	0.628	0.908	3.284	0.148	0.948	1.315	0.123	0.952
Cpd (2)	1.704	2.141	0.919	3.03	0.132	0.942	2.869	0.117	0.981
Cpd (3)	0.023	0.615	0.965	1.429	0.117	0.982	0.478	0.22	0.992
Cpd (4)	0.268	0.514	0.978	2.158	0.144	0.98	0.84	0.166	0.996
Cpd (5)	1.165	0.49	0.901	0.638	0.067	0.991	0.914	0.26	0.972
Cpd (6)	0.745	0.495	0.972	1.374	0.061	0.997	0.35	0.265	0.991

Table 2. Kinetic model constants of adsorbed metal ions onto blank and modified p(AAm-co-AAc) hydrogels.

size distribution and overall porosity of the adsorbent material can also affect the accessibility and diffusion of metal ions into the material. Samples with more prominent pores or higher porosity may provide better access to the adsorption sites, resulting in higher β values. Conversely, samples with smaller pores or lower porosity may have restricted diffusion, leading to lower β values. Besides, the surface chemistry of the adsorbent can influence the electrostatic interactions and chemical reactions among the adsorbent and metal ions.

The above kinetic results highlight the influence of the modification strategies on the adsorption kinetics and effectiveness of hydrogel for different metal ions. This further indicates that the adsorption is primarily driven by van der Waals forces and electrostatic interactions among the adsorbent surface and the metal ions in the solution³⁷. The sharing or trading of electrons among the hydrogel functionalities ($-\text{SO}_3^-$ and $-\text{COO}^-$) and the HMs cations results in the involvement of the valent forces. The existence of additional exchangeable groups resulting from the chemical modification approach of the hydrogel likely enhances the adsorption performance, as evidenced by the higher removal rates observed for Cu^{2+} and Ba^{2+} ions compared to that obtained by the blank p(AAm-co-AAc) hydrogel (Cpd0) sample. This modification approach introduces more binding sites on the hydrogel surface, increasing the availability of active sites for metal ion adsorption by sharing or exchanging electrons among adsorbent and adsorbate³⁸.

Effect of adsorption temperature: thermodynamic study

Understanding the thermodynamic behavior can provide valuable insights into the energetics of the adsorption approach and help optimize conditions for efficient metal ion removal in practical applications. Figure 7 shows that the adsorption of Cu^{2+} and Ba^{2+} onto the modified and bare p(AAm-co-AAc) adsorbents is favored at higher temperatures. An increase in the temperature enhances the adsorption processes of Cu^{2+} and Ba^{2+} , owing to their favorable endothermic adsorption. In this case, the higher temperature provides the necessary energy for adsorption and facilitates the interaction between metal ions and adsorbent surfaces. On the other hand, the adsorption of Sr^{2+} onto Cpd3, Cpd5, and Cpd6 is significantly declined as the temperature rises (i.e., an exothermic adsorption nature). This phenomenon can be attributed to the thermodynamic characteristics of the adsorption process, where the energy released during adsorption is sufficient to counteract the increased thermal energy at higher temperatures.

To further understand the adsorption thermodynamics, the thermodynamic parameters of the three metal ions onto the prepared hydrogel adsorbent are calculated using the Eq. (9). The plot of $\ln K_D$ against $1/T$ will be used to calculate ΔH° , as shown in Fig. 8. It should be noted that a spontaneous system will display a decrease in ΔG° and ΔH° values with increasing temperature³⁹.

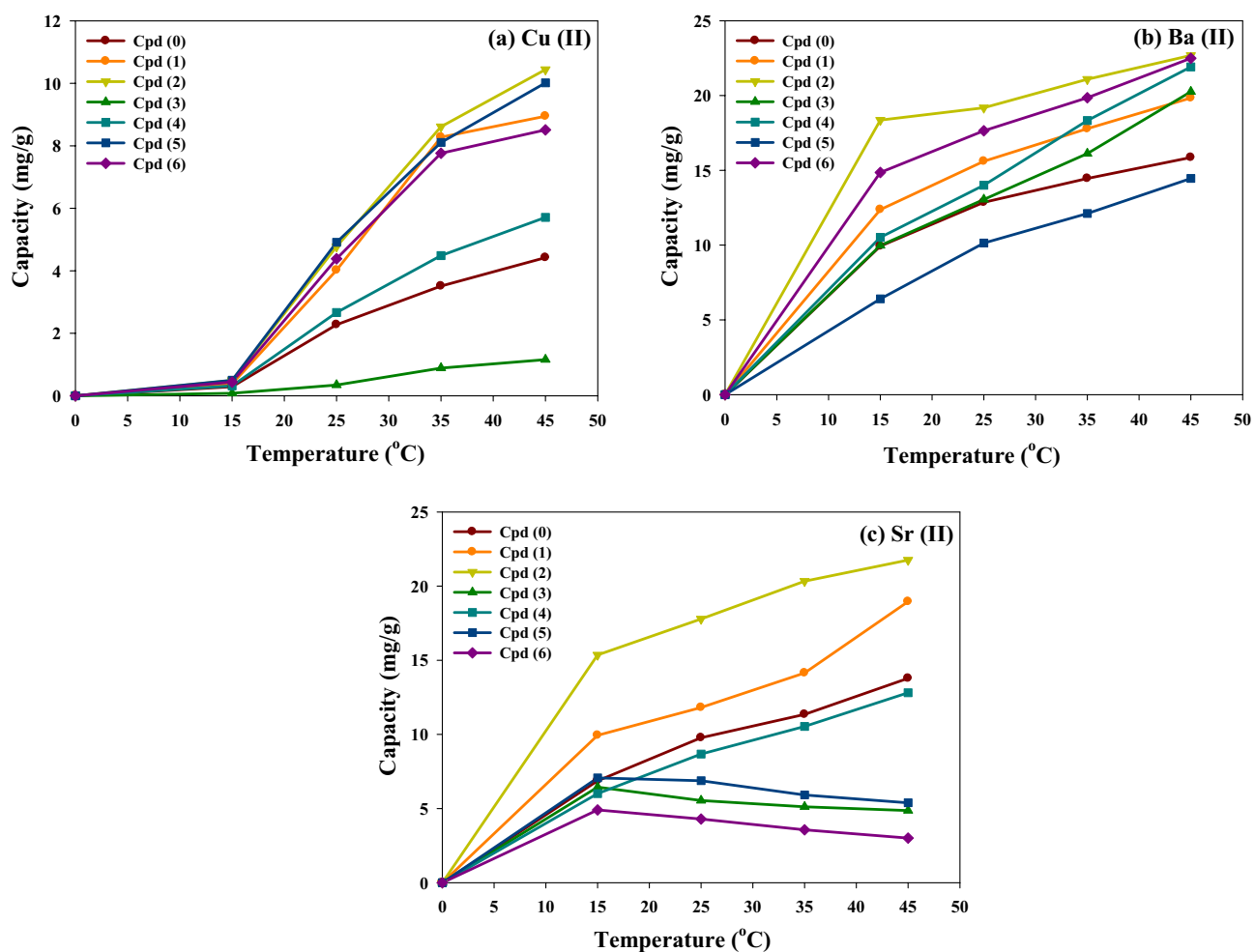


Figure 7. The impact of temperature on the adsorption capacity of three metal ions by p(AAm-co-AAc) hydrogels before and after functionalization processes.

$$\ln K_D = \frac{\Delta S}{R} - \frac{\Delta H}{RT} \quad (9)$$

- $\ln K_D$: This represents the natural logarithm of the equilibrium constant. The equilibrium constant measures the extent to which a chemical reaction reaches equilibrium, indicating the ratio of products to reactants at equilibrium.
- ΔS : This term represents the change in entropy of the system. Entropy is a measure of the disorder or randomness of a system. A positive ΔS value suggests an increase in randomness, while a negative value suggests a decrease.
- R : The gas constant (0.08314 kJ/(mol·K)) is a fundamental thermodynamic constant.
- ΔH : This term represents the change in enthalpy of the system. Enthalpy measures the heat energy absorbed or released during a chemical reaction. A negative ΔH value suggests an exothermic reaction (heat released), while a positive value suggests an endothermic reaction (heat absorbed).
- T : The temperature of the system in Kelvin (K).

Table 3 presents the thermodynamic constants of the three adsorbed metal ions by blank and modified hydrogels based on Van't Hoff plots in Fig. 8. As can be noticed, the positive ΔH° values for Cu^{2+} , Ba^{2+} , and Sr^{2+} metal ions adsorption indicate that the adsorption process is endothermic. An exception is the adsorption process of Sr^{2+} ions by Cpd3, Cpd5, and Cpd6, which recorded negative ΔH° values (i.e., exothermic adsorption process). Depending on the specific hydrogel samples, the positive and negative values of ΔH° for Sr^{2+} adsorption suggest both exothermic and endothermic processes. The endothermic adsorption verified the crucial role of temperature in enhancing metal ions' adsorption uptake, especially Cu^{2+} , which needs higher activation energy to induce chelating/complex interactions with hydrogel surface functionalities. For Cu^{2+} adsorption, the ΔH° values ranged from 25.39 kJ/mol (Cpd0) to 92.88 kJ/mol (Cpd2), demonstrating the dominant chemical adsorption mechanism. However, for $\text{Ba}^{2+}/\text{Sr}^{2+}$ ions adsorption, the low adsorption enthalpy (ΔH° less than 60 kJ/mol) indicates that their adsorption behaviors are particular and involve physical and weak chemical adsorption interactions with

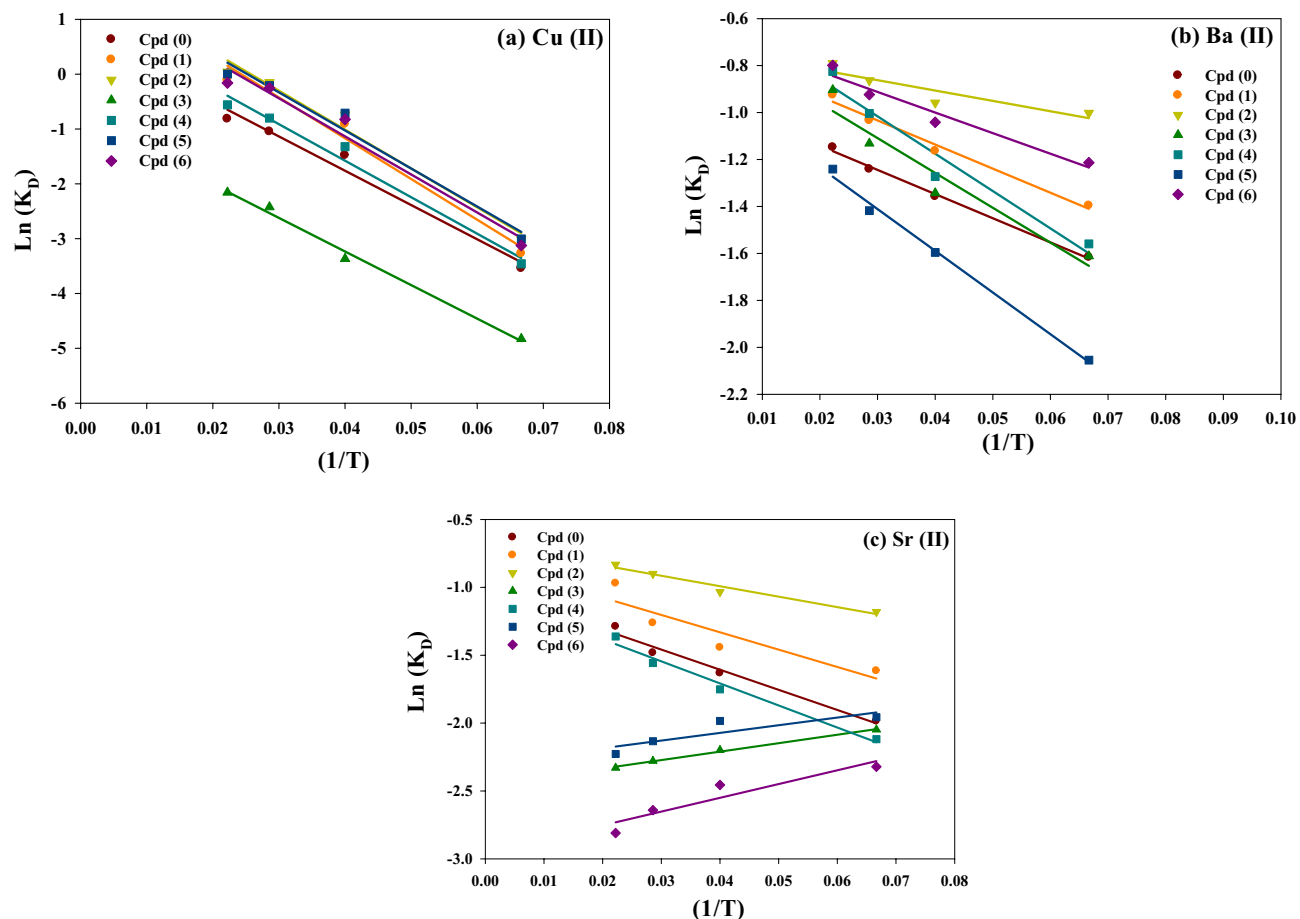


Figure 8. Graphical relationship plots between $\ln K_D$ and $1/T$ to determine the enthalpy change (ΔH°) of (a) Cu^{2+} , (b) Ba^{2+} , and (c) Sr^{2+} ions adsorbed by the prepared hydrogel adsorbents.

Hydrogels/Constants*	Cu^{2+}			Ba^{2+}			Sr^{2+}		
	ΔH°	ΔS°	ΔG°	ΔH°	ΔS°	ΔG°	ΔH°	ΔS°	ΔG°
Cpd (0)	25.39	0.08	2.16	24.17	0.08	1.57	28.91	0.09	2.82
Cpd (1)	80.37	0.28	-1.78	34.25	0.11	0.46	38.14	0.12	1.99
Cpd (2)	92.88	0.33	-5.85	32.42	0.11	-1.24	37.17	0.13	-0.52
Cpd (3)	62.55	0.18	8.16	46.17	0.15	1.50	-9.12	-0.05	4.83
Cpd (4)	32.01	0.10	1.39	57.68	0.19	1.12	29.87	0.09	3.28
Cpd (5)	55.47	0.22	-8.19	34.13	0.10	2.67	-9.70	-0.05	4.12
Cpd (6)	56.03	0.20	-3.15	44.80	0.15	-0.45	-14.86	-0.07	5.62

Table 3. The thermodynamic parameters (ΔH° , ΔG° , and ΔS°)* of the three adsorbed metal ions onto the blank and modified hydrogel adsorbents. *Thermodynamic constants: Standard enthalpy change (ΔH : kJ/mol), Free energy change (ΔG : kJ/mol), and Entropy change (ΔS : kJ/mol.K).

hydrogel surface functionalities. The exothermic adsorption of Sr^{2+} ions by Cpd3, Cpd5, and Cpd6 indicates stronger adsorbate-adsorbent interactions with heat released during the adsorption process. In contrast, the enhanced adsorption of metal ions with temperature could be ascribed to the improved mass transfer/diffusivity rate through the hydrogel porous networks. The variation in ΔH° values across different samples highlights the influence of the adsorbent composition on the adsorption behavior of each metal ion. These thermodynamic parameters provide insights into the energetics of the adsorption process, indicating the strength and nature of the interaction between the metal ions and the adsorbent. The positive ΔS° values for metal ions also indicate the rise in randomness at the liquid–solid interface during adsorption. This randomness increases with increased metal ion activity in water and their interactions with adsorbent surface sites. The variation in the ΔG° (negative and positive values) also indicates the thermodynamic feasibility of the adsorption process, and the adsorption interaction is less favorable at lower temperatures. These findings highlight the importance of considering the

thermodynamic aspects of the adsorption process, particularly the exothermic or endothermic nature, when studying the adsorption of different metal ions onto specific adsorbents.

The above thermodynamic data are further verified by the calculated activation energies (E_a) for the adsorption of Cu^{2+} , Ba^{2+} , and Sr^{2+} ions by the modified p(AAm-co-AAc) hydrogels using the Arrhenius equation: $k = A e^{(-E_a/RT)}$, where k is rate constant, A is pre-exponential factor, E_a is activation energy (kJ/mol) by taking the natural log of the Arrhenius equation. $\ln(k) = \ln(A) - (E_a/R)(1/T)$. A plot of $\ln(k)$ vs $1/T$ will give a straight line with slope = $-E_a/R$. From this slope, the activation energy E_a can be calculated and summarized in Table 4. These values represent the energy required for the adsorption process to take place. Lower activation energies indicate that adsorption is more favorable and occurs more quickly. Conversely, higher activation energies suggest that adsorption is less favorable and requires more energy. The specific values provide insights into the adsorption behavior of these metal ions on the different hydrogel samples. For instance, in most cases, Cu^{2+} ions show higher activation energies, suggesting a higher energy barrier for their adsorption. Ba^{2+} ions exhibit relatively lower activation energies, making them easier to adsorb.

Comparative study

Table 5 shows the comparative adsorption capacities of different adsorbents for removing Cu^{2+} , Ba^{2+} and Sr^{2+} from water. Modified fly ash and graphene oxide sheets showed Cu^{2+} removal capacities of 53.5 mg/g and 46.6 mg/g, respectively. Polyethylene glycol diacrylate-3-sulfopropyl methacrylate potassium salt exhibited the highest Cu adsorption capacity of 99 mg/g. Magnetic chitosan beads and hydroxyapatite were effective for Sr^{2+} removal with capacities of 11.58 mg/g and 28.51 mg/g, respectively. titanium silicate and $\text{TiY}_2\text{O}_5@g\text{-C}_3\text{N}_4$ had high Ba^{2+} adsorption of 144 mg/g and 295 mg/g. Allophane showed 38.6 mg/g and 34.4 mg/g capacities for Ba^{2+} and Sr^{2+} , respectively. P(CTS-AAm) and Chitosan-g-maleic acid had excellent Cu removal of 196.8 mg/g and 312.4 mg/g. The present work showed relatively lower but significant capacities of 13.67 mg/g, 36.4 mg/g and 27.31 mg/g for Cu^{2+} , Ba^{2+} and Sr^{2+} removal in 1000 ppm of NaCl solution. Thus different low-cost adsorbents can be effectively used for heavy metal remediation from water.

Sample	Cu^{2+} E_a (kJ/mol)	Ba^{2+} E_a (kJ/mol)	Sr^{2+} E_a (kJ/mol)
Cpd (0)	59.7	53.2	56.1
Cpd (1)	63.2	57.6	58.9
Cpd (2)	71.5	50.8	55.6
Cpd (3)	58.4	55.1	61.7
Cpd (4)	60.9	59.6	59.2
Cpd (5)	64.8	56.3	63.5
Cpd (6)	64.1	49.5	57.8

Table 4. The activation energies (E_a : kJ/mol) for the adsorption of Cu^{2+} , Ba^{2+} , and Sr^{2+} ions by the blank and modified p(AAm-co-AAc) hydrogel adsorbents.

Adsorbent	Cu^{2+} (mg/g)	Ba^{2+} (mg/g)	Sr^{2+} (mg/g)	Ref
Modified fly ash	53.5	N/A	N/A	40
Modified graphene oxide (GO) sheets	46.6	N/A	N/A	41
Polyethylene glycol diacrylate-3-sulfopropyl methacrylate potassium salt (PEGDA-SMP)	99	N/A	N/A	42
Magnetic chitosan beads	N/A	N/A	11.58	43
Alkali activated metakaolin	N/A	N/A	167.5	44
Hydroxyapatite	N/A	N/A	28.51	45
Titanium silicate	N/A	144	N/A	46
$\text{TiY}_2\text{O}_5@g\text{-C}_3\text{N}_4$	N/A	295	N/A	47
Allophane	N/A	38.6	34.4	48
P(CTS-AAm)	196.8	N/A	N/A	49
Chitosan-g-maleic acid	312.4	N/A	N/A	50
Present work	13.67	36.4	27.31	In 1000 PPM of NaCl

Table 5. Comparative of different adsorbents for adsorption removal of Cu^{2+} , Ba^{2+} , and Sr^{2+} ions from water solution.

Conclusions

The radiation synthesis of p(AAm-co-AAc) adsorbents is based on chemically developed for the removal of three metal ions (Cu^{2+} , Ba^{2+} , and Sr^{2+}) from a synthetic saline solution (NaCl 1000 ppm) is successively performance. The observed trend suggests that co-monomer concentration can be optimized to achieve the desired application swelling properties. Lower co-monomer concentrations can be preferred when high swelling capacity is required, while higher concentrations can be suitable for a more compact and less-swelling hydrogel. The swelling degrees of the prepared p(AAm-co-AAc) hydrogels are lower when the acrylic acid content is higher than those with higher polyacrylamide content. The lower swelling degrees of hydrogels with higher acrylic acid content can be attributed to intermolecular hydrogen bonds formed by acrylic acid molecules, which restrict the uptake of water molecules by the hydrogel, leading to a decrease in swelling capacity. Further investigation and optimization of irradiation dose can help tailor hydrogel properties for specific applications requiring controlled swelling behavior and mechanical strength. Variations in pore diameter and hydrogel wall thickness are observed in the modified samples. Hydrogels with stronger hydrogen bonding exhibit smaller pore sizes, while those with weaker hydrogen bonding show larger pore sizes. During the adsorption process, it was also found that the adsorption performance of p(AAm-co-AAc) hydrogel depends mainly on the modifying agent and the specific HM ion being targeted (e.g., Cu^{2+} , Ba^{2+} , and Sr^{2+}). Adsorption results showed that the chemically modified hydrogel with sodium hydroxide (Cpd 2) exhibited the highest affinity for the adsorption recovery of the three HM ions. Based on adsorption isotherm, kinetic, and thermodynamic studies, the adsorption process of Cu^{2+} , Ba^{2+} , and Sr^{2+} ions onto the modified p(AAm-co-AAc) hydrogel samples followed a favorable multilayer adsorption mechanism, especially at higher temperature. The adsorption energy also indicates the dominance of chemical interaction between Cu ions and hydrogel surface functionalities, while the adsorption of Ba^{2+} and Sr^{2+} ions involves moderate to strong adsorption interactions, including a complex physicochemical adsorption phenomenon. These adsorption data can contribute to further understanding the suitability and effectiveness of these hydrogels as adsorbents for metal ion removal in various applications (Supplementary Information).

Data availability

The data that support the findings of this study are available from the corresponding author upon reasonable request.

Received: 19 September 2023; Accepted: 2 December 2023

Published online: 11 December 2023

References

- Chen, X., Di, Q., Jia, W. & Hou, Z. Spatial correlation network of pollution and carbon emission reductions coupled with high-quality economic development in three Chinese urban agglomerations. *Sustain. Cities Soc.* **94**, 104552 (2023).
- Prasad, M. & Suresh, L. Another side of industrial growth in India: Environmental damage from industrial accidents. *Saf. Sci.* **164**, 106152 (2023).
- Fei, Y. & Hu, Y. H. Recent progress in removal of heavy metals from wastewater: A comprehensive review. *Chemosphere* **335**, 139077 (2023).
- Lee, Y. H. *et al.* Organelle-selective fluorescent Cu²⁺ ion probes: Revealing the endoplasmic reticulum as a reservoir for Cu-overloading. *Chem. Commun.* **50**, 3197–3200 (2014).
- Amoatey, P. & Baawain, M. S. Effects of pollution on freshwater aquatic organisms. *Water Environ. Res.* **91**, 1272–1287 (2019).
- Peana, M. *et al.* Environmental barium: Potential exposure and health-hazards. *Arch. Toxicol.* **95**, 2605–2612 (2021).
- Gould, J. M. *et al.* Strontium-90 in deciduous teeth as a factor in early childhood cancer. *Int. J. Health Serv.* **30**, 515–539 (2000).
- Mishra, S. *et al.* Heavy metal contamination: An alarming threat to environment and human health. In *Environmental Biotechnology: For Sustainable Future* (eds Sobti, R. C. *et al.*) 103–125 (Springer Singapore, 2019).
- Gokul, T. *et al.* Impact of particulate pollution on aquatic invertebrates. *Environ. Toxicol. Pharmacol.* **100**, 104146 (2023).
- Rashid, R., Shafiq, I., Akhter, P., Iqbal, M. J. & Hussain, M. A state-of-the-art review on wastewater treatment techniques: The effectiveness of adsorption method. *Environ. Sci. Pollut. Res.* **28**, 9050–9066 (2021).
- Huang, L. *et al.* Research progresses on the application of perovskite in adsorption and photocatalytic removal of water pollutants. *J. Hazard. Mater.* **442**, 130024 (2023).
- Ghobashy, M. M. *Hydrogels Based on Natural Polymers* 329–356 (Elsevier, 2020).
- Maksoud, M. I. A. A., Youssef, M. A., Ghobashy, M. M., Aly, M. I. & Ashour, A. H. Gamma radiation-induced synthesis of organo-clays based polyaniline and ilmenite clay minerals for cesium ions removal from aqueous solutions. *Separat. Purif. Technol.* **305**, 122434 (2023).
- Alkhursani, S. A. *et al.* Application of nano-inspired scaffolds-based biopolymer hydrogel for bone and periodontal tissue regeneration. *Polymers* **14**, 3791 (2022).
- Atia, G. A. N. *et al.* Drug-loaded chitosan scaffolds for periodontal tissue regeneration. *Polymers* **14**, 3192 (2022).
- Ghobashy, M. M. *et al.* Controlling radiation degradation of a CMC solution to optimize the swelling of acrylic acid hydrogel as water and fertilizer carriers. *Polym. Adv. Technol.* **32**, 514–524 (2021).
- Ghobashy, M. M. *et al.* Improvement of in vitro dissolution of the poor water-soluble amlodipine drug by solid dispersion with irradiated polyvinylpyrrolidone. *ACS Omega* **5**, 21476–21487 (2020).
- Ghobashy, M. M., El-Sawy, N. M. & Kodous, A. S. Nanocomposite of cosubstituted carbonated hydroxyapatite fabricated inside Poly (sodium hyaluronate-acrylamide) hydrogel template prepared by gamma radiation for osteoblast cell regeneration. *Radiat. Phys. Chem.* **183**, 109408 (2021).
- Alshangiti, D. M. *et al.* Semi-permeable membrane fabricated from organoclay/PS/EVA irradiated by γ -rays for water purification from dyes. *J. Mater. Res. Technol.* **8**, 6134–6145 (2019).
- Ghobashy, M. M., Reheem, A. M. A. & Mazied, N. A. Ion etching induced surface patterns of blend polymer (poly ethylene glycol-poly methyl methacrylate) irradiated with gamma rays. *Int. Polymer Process.* **32**, 174–182 (2017).
- Madani, M. *et al.* Green synthesis of nanoparticles for varied applications: Green renewable resources and energy-efficient synthetic routes. *Nanotechnol. Rev.* **11**, 731–759 (2022).
- Younis, S. A., Ghobashy, M. M., Bassioni, G. & Gupta, A. K. Tailored functionalized polymer nanoparticles using gamma radiation for selected adsorption of barium and strontium in oilfield wastewater. *Arab. J. Chem.* **13**, 3762–3774 (2020).
- Akram, M., Taha, I. & Ghobashy, M. M. Low temperature pyrolysis of carboxymethylcellulose. *Cellulose* **23**, 1713–1724 (2016).

24. Ghobashy, M. M. *et al.* Optimal the mechanical properties of bioplastic blend based algae-(lactic acid-starch) using gamma irradiation and their possibility to use as compostable and soil conditioner. *Mater. Today Commun.* **34**, 105472 (2023).
25. Sinha, V. & Chakma, S. Advances in the preparation of hydrogel for wastewater treatment: A concise review. *J. Environ. Chem. Eng.* **7**, 103295 (2019).
26. Zhang, K., Luo, X., Yang, L., Chang, Z. & Luo, S. Progress toward hydrogels in removing heavy metals from water: Problems and solutions—A review. *ACS ES&T Water* **1**, 1098–1116 (2021).
27. Zhao, B. *et al.* Preparation of acrylamide/acrylic acid cellulose hydrogels for the adsorption of heavy metal ions. *Carbohydr. Polymers* **224**, 115022 (2019).
28. Zhang, M. *et al.* High crosslinked sodium carboxyl methylstarch-g-poly (acrylic acid-co-acrylamide) resin for heavy metal adsorption: Its characteristics and mechanisms. *Environ. Sci. Pollut. Res.* **27**, 38617–38630 (2020).
29. Sun, Z. *et al.* A novel modified carboxymethyl cellulose hydrogel adsorbent for efficient removal of poisonous metals from wastewater: Performance and mechanism. *J. Environ. Chem. Eng.* **10**, 108179 (2022).
30. Pérez-Calderón, J., Santos, M. V. & Zaritzky, N. Synthesis, characterization and application of cross-linked chitosan/oxalic acid hydrogels to improve azo dye (Reactive Red 195) adsorption. *Reactive Funct. Polymers* **155**, 104699 (2020).
31. Shen, J., Xu, X., Ouyang, X.-k. & Jin, M.-c. Adsorption of Pb (II) from aqueous solutions using nanocrystalline cellulose/sodium alginate/K-carrageenan composite hydrogel beads. *J. Polymers Environ.* 1–12 (2022).
32. Guo, S., Yuan, S., Geng, W. & Dong, Z. Preparation and optimization of thermosensitive hydrogels for inhibiting coal oxidation. *Int. J. Energy Res.* **45**, 7783–7796 (2021).
33. Pawlukojć, A., Leciejewicz, J., Ramirez-Cuesta, A. J. & Nowicka-Scheibe, J. L-Cysteine: Neutron spectroscopy, Raman, IR and ab initio study. *Spectrochim. Acta A Mol. Biomol. Spectroscopy* **61**, 2474–2481 (2005).
34. Trivedi, J. H., Min, W., Huang, Y. & Trivedi, H. C. Photo-induced sodium salt of partially carboxymethylated psyllium-g-polyacrylonitrile: II. Synthesis, characterization and swelling behaviour of its superabsorbent hydrogel. *Int. J. Sci. Res. Publ.* **5**, 1–10 (2015).
35. Foo, K. Y. & Hameed, B. H. Insights into the modeling of adsorption isotherm systems. *Chem. Eng. J.* **156**, 2–10 (2010).
36. Wang, J. & Guo, X. Adsorption kinetic models: Physical meanings, applications, and solving methods. *J. Hazard. Mater.* **390**, 122156 (2020).
37. Al-Ghouthi, M., Khraisheh, M. A. M., Ahmad, M. N. M. & Allen, S. Thermodynamic behaviour and the effect of temperature on the removal of dyes from aqueous solution using modified diatomite: a kinetic study. *J. Colloid Interface Sci.* **287**, 6–13 (2005).
38. Mayakaduwa, S. S. *et al.* Equilibrium and kinetic mechanisms of woody biochar on aqueous glyphosate removal. *Chemosphere* **144**, 2516–2521 (2016).
39. Ibrahim, A. G., Sayed, A. Z., Abd El-Wahab, H. & Sayah, M. M. Synthesis of a hydrogel by grafting of acrylamide-co-sodium methacrylate onto chitosan for effective adsorption of Fuchsin basic dye. *Int. J. Biol. Macromol.* **159**, 422–432 (2020).
40. Buema, G., Trifas, L.-M. & Harja, M. Removal of toxic copper ion from aqueous media by adsorption on fly ash-derived zeolites: Kinetic and equilibrium studies. *Polymers* **13**, 3468 (2021).
41. Tan, P. *et al.* Adsorption of Cu²⁺, Cd²⁺ and Ni²⁺ from aqueous single metal solutions on graphene oxide membranes. *J. Hazard. Mater.* **297**, 251–260 (2015).
42. Dharmapriya, T. N., Li, D., Chung, Y.-C. & Huang, P.-J. Green synthesis of reusable adsorbents for the removal of heavy metal ions. *ACS Omega* **6**, 30478–30487 (2021).
43. Chen, Y. & Wang, J. Removal of radionuclide Sr²⁺ ions from aqueous solution using synthesized magnetic chitosan beads. *Nuclear Eng. Des.* **242**, 445–451 (2012).
44. Huang, Y.-H. & Wu, Y.-C. Highly efficient adsorption of Sr²⁺ and Co²⁺ ions by ambient prepared alkali activated metakaolin. *Polymers* **14**, 992 (2022).
45. Kim, J., Sambudi, N. S. & Cho, K. Removal of Sr²⁺ using high-surface-area hydroxyapatite synthesized by non-additive in-situ precipitation. *J. Environ. Manag.* **231**, 788–794 (2019).
46. Savka, K. *et al.* Ba²⁺ ions adsorption by titanium silicate. *Chem. Phys. Impact* **6**, 100151 (2023).
47. Modwi, A. *et al.* Ba²⁺ removal from aquatic medium via TiY₂O₅@g-C₃N₄ nanocomposites. *Diamond Related Mater.* **135**, 109830 (2023).
48. Baldermann, A. *et al.* Removal of barium, cobalt, strontium, and zinc from solution by natural and synthetic allophane adsorbents. *Geosciences* **8**, 309 (2018).
49. Saleh, A. S. *et al.* Preparation of poly (chitosan-acrylamide) flocculant using gamma radiation for adsorption of Cu (II) and Ni (II) ions. *Radiat. Phys. Chem.* **134**, 33–39 (2017).
50. Ibrahim, A. G., Saleh, A. S., Elsharma, E. M., Metwally, E. & Siyam, T. Chitosan-g-maleic acid for effective removal of copper and nickel ions from their solutions. *Int. J. Biol. Macromol.* **121**, 1287–1294 (2019).

Acknowledgements

The authors acknowledge all support given by both the Faculty of Engineering and Faculty of Science at Ain Shams University, the City of Scientific Research and Technological Applications (SRTA-City), the Egyptian Petroleum Research Institute (EPRI), and the National Center for Radiation Research and Technology (NCRRT) to conduct all experimental studies and characterization made in this cooperative research work.

Author contributions

I.K.A.M.: Data curation, Investigation, Methodology, Writing—original draft, and SEM analysis. G.B.: Data curation, Investigation, Writing—review & editing. N.N.: Data curation, Methodology, Writing—review & editing. S.A.Y.: Conceptualization, Data curation, Investigation, Methodology, Resources, Formal analysis, Validation, Visualization, Writing—original draft, Writing—review & editing. M.M.G.: Hydrogel preparation, hydrogel modification, FTIR analysis, Data curation, Validation, Methodology, Resources, Writing—original draft, Writing—review & editing. M.S.A.A.-M.: Data curation, Writing—review & editing, Supervision.

Funding

Open access funding provided by The Science, Technology & Innovation Funding Authority (STDF) in cooperation with The Egyptian Knowledge Bank (EKB).

Competing interests

The authors declare no competing interests.

Additional information

Supplementary Information The online version contains supplementary material available at <https://doi.org/10.1038/s41598-023-49009-0>.

Correspondence and requests for materials should be addressed to S.A.Y. or M.M.G.

Reprints and permissions information is available at www.nature.com/reprints.

Publisher's note Springer Nature remains neutral with regard to jurisdictional claims in published maps and institutional affiliations.



Open Access This article is licensed under a Creative Commons Attribution 4.0 International License, which permits use, sharing, adaptation, distribution and reproduction in any medium or format, as long as you give appropriate credit to the original author(s) and the source, provide a link to the Creative Commons licence, and indicate if changes were made. The images or other third party material in this article are included in the article's Creative Commons licence, unless indicated otherwise in a credit line to the material. If material is not included in the article's Creative Commons licence and your intended use is not permitted by statutory regulation or exceeds the permitted use, you will need to obtain permission directly from the copyright holder. To view a copy of this licence, visit <http://creativecommons.org/licenses/by/4.0/>.

© The Author(s) 2023